1-1-2014

Identifying the Vulnerability of Earthen Levees to Slump Slides using Geotechnical and Geomorphological Parameters

Sona Sehat

Identifying the vulnerability of earthen levees to slump slides using geotechnical and geomorphological parameters

By

Sona Sehat

A Thesis
Submitted to the Faculty of
Mississippi State University
in Partial Fulfillment of the Requirements
for the Degree of Master of Science
in Civil Engineering
in the Department of Civil and Environmental Engineering

Mississippi State, Mississippi

December 2014

Identifying the vulnerability of earthen levees to slump slides using geotechnical and geomorphological parameters

By

Sona Sehat

Approved:

_____

Farshid Vahedifard
(Major Professor)

_____

James V. Aanstoos
(Committee Member)

_____

Dennis D. Truax
(Committee Member)

_____

James L. Martin
(Graduate Coordinator)

_____

Jason M. Keith
Interim Dean
Bagley College of Engineering

Name: Sona Sehat

Date of Degree: December 13, 2014

Institution: Mississippi State University

Major Field: Civil Engineering

Major Professor: Dr. Farshid Vahedifard

Title of Study: Identifying the vulnerability of earthen levees to slump slides using geotechnical and geomorphological parameters

Pages in Study: 81

Candidate for Degree of Master of Science

The main goal of this research is to investigate vulnerability of levees to future slump slides. In the first part, polarimetric synthetic aperture radar (PolSAR) imagery is used as input in an automated classification system for characterizing areas on the levee having anomalies. In addition, a set of in-situ soil data is collected to provide detailed soil properties over the study area. In-situ soil properties of different classes characterized by the classifier are analyzed to determine how similarities between different areas. The second part, a database including of 34 slump slides that occurred in the lower Mississippi River levee system over a period of two years is used. The impacts of rainfall as well as several spatial geometrical and geomorphological variables (including channel width, river sinuosity index, riverbank erosion, channel shape condition and distance to river) are analyzed and tested for significance and used for developing a logistic regression model.

DEDICATION

To those who fight for freedom…

ACKNOWLEDGEMENTS

I would like to express my deep gratitude to my advisor Dr. Farshid Vahedifard for his honest support of my study and research, for his patience, enthusiasm, excellent knowledge. I am so lucky that he is not just a teacher to me, but also a true friend.

I would like to thank my thesis committee: Prof. Dennis D. Truax and Prof. James V. Aanstoos, for their kindness, supports, encouragements, and patience. Also, I would like to appreciate all the supports that Dr. Aanstoos provided in the past two years for our project.

I thank my colleagues in High Performance Computing Collaboratory (HPC^2): Dr. Khaled Hasan and Ms. Lalitha Dabbiru for all the helpful discussions, their support and patience.

Last but not least, I would like to thank my parents for supporting me throughout the course of my life, and for training me to be who I am today.

TABLE OF CONTENTS

LIST OF TABLES

LIST OF FIGURES

CHAPTER I

INTRODUCTION

Background

Over 160,000 km of federal and non-federal earthen levees provide flood protection in different regions of the United States (CRS, 2011). Failure of levees due to natural hazards such as floods or earthquakes causes catastrophic damage and loss of life. Various phenomena may lead to levee breach including: overtopping, sand boils and hydraulic soil failure and loss of levee stability (Bogardi & Mathe, 1968). Erosion of levees due to seepage through the body, seepage under the levee body (i.e., underseepage), or saturation of materials in the levee body and loss of soil stability are considered as structural failure. Erosion in levees with cohesive soils may occur due to existence of cracks and/or hydraulic fractures caused by differential settlement during construction or operation, and/or low stresses near conduits or due to high level desiccation in the fill (Fell & Fry, 2013). Among different modes of failure in levees, seepage and underseepage are crucial factors for distress conditions. They can negatively affect slope stability by reducing effective stresses in the levee body and foundation soil (Bhowmik et al., 1994; Flor et al., 2010).

On the other hand, less severe events such as slump slides can also threaten the integrity of levees. Slump slides are relatively shallow surficial instabilities on the river-side of levees which usually occur after a heavy rainfall with a long period of drying

(Sills, 1983). This cycle of wetting and drying reduces the soil strength, and the excess water triggers the slump slide (Hossain et al., 2006). Such slump slides occur frequently along the Mississippi River levees.

Objectives

The main objective of the study outlined in this research is to investigate methods that can be used to identify high risk and vulnerable areas to future slump slides on levees in order to take immediate protective actions, closer monitoring and early response under emergency conditions.

The first goal of this research is to improve the accuracy of the current levee monitoring system by validating the potential of a remote sensing-based model for detecting slump slide failures. To accomplish this task, the imagery acquired by the NASA Uninhabited Aerial Vehicle Synthetic Aperture Radar (UAVSAR) from January 25, 2010 was used as an input in the Reed-Xiaoli Detector (RXD) classifier algorithm (Reed and Yu, 1990) along with in situ measurements of a variety of soil properties. While the automated classification system correctly identified the location of active slides, there were some points, referred to as “false positive points”, which were classified as anomalous but no failure was found at those locations. The goal was to investigate the vulnerability of false positive points from this unsupervised levee slump slide classifier to future failures by comparing in-situ soil properties of the false positive points with those of true positive points (i.e., the slide area) and true negatives (i.e., the healthy areas) to determine how similar they are to either the healthy or slide areas.

The second goal of this research is to investigate the relevance and importance of rainfall and various geometrical and geomorphological factors to the vulnerability of

earthen levees to slump slides using a dataset from 34 slump slides that occurred in the lower Mississippi River levee system over a period of two years. To accomplish this task, monthly and cumulative monthly precipitation are plotted for each slump slide to qualitatively test the importance of rainfall gradient in the ultimate slump slide failure. In addition, multiple spatial variables, including channel width, river sinuosity index, riverbank erosion, channel shape condition and distance to river are used in a logistic regression model to investigate their impact on slump slide occurrence on levees.

Scope

The first part of this research examines false positive points by comparing their soil properties with those of the active slump slide and healthy areas on a 1.7 km long levee system of the Lower Mississippi River to investigate if they have any similarity to either of these areas. Any slope stability analysis for suspected areas as well as huge levee failure analysis is beyond the scope of this work.

In the second part, the relevance and importance of rainfall and various geometrical and geomorphological factors are investigated to the vulnerability of more than 170 km of Lower Mississippi River levee system to slump slides. The study is performed using data from 34 slump slides that occurred in the lower Mississippi River levee system over a time period of two years. The scope of this part includes conducting qualitative analysis of monthly rainfall and performing a set of logistic regression analyses to find the relevance of five factors including channel width, channel sinuosity index, riverbank erosion, channel shape condition and distance to river.

Contribution

This study is implemented on the main levee system of the Lower Mississippi River. The major contributions from this research are:

The errors from a classifier's output known as "errors of commission" or "false positive points" are validated by analyzing soil properties on the levee, and the results indicate further attention and monitoring at the locations with a high spatial density of false positive points are strongly recommended.

The effects of monthly rainfall in the six months prior to the slump slide events are studied. Moreover, the importance of geological and geomorphological parameters on the vulnerability of levees to slump slide is analyzed; low channel width and riverbank erosion are found to be high risk areas for slump slide vulnerability on levees in this study area.

CHAPTER II

USING IN SITU SOIL MEASUREMENTS FOR ANALYSIS OF A POLARIMETRIC SAR-BASED CLASSIFICATION OF LEVEE SLUMP SLIDES IN THE LOWER MISSISSIPPI RIVER

Introduction

Over 160,000 km of federal and non-federal earthen levees provide flood protection in different regions of the United States (CRS 2011). Failure of levees due to natural hazards such as floods or earthquakes causes catastrophic damage and loss of life. In the United States, among 744 levees that were listed in the National Levee Database (NDL) only 10% were rated "acceptable" which means the levee was found in "satisfactory condition". The rest were rated "minimally acceptable" (79%) or "unacceptable" (11%) indicating the levee has a minor deficiency or the levee cannot serve as a reliable flood protection structure, respectively (Maciag, 2011). Many of these unacceptable-rated levees are almost 70 years old (NRC, 2012). Catastrophic failures of levees in the Midwest and along the Mississippi River and in New Orleans during hurricane Katrina are examples of this problem. Even after spending over $14 billion dollars on raising, reconstructing and reinforcing levees in the New Orleans area, the U.S. Army Corps of Engineers (USACE) admits that the new system still may not fully protect New Orleans against future events (Reid, 2013).

As demonstrated in Fig. 1, various phenomena may lead to levee failure including: overtopping, sand boils and hydraulic soil failure and loss of levee stability (Bogardi & Mathe, 1968). Erosion of levees due to seepage through the body, seepage under the levee body (i.e., underseepage), or saturation of materials in the levee body and loss of soil stability are considered as structural failure. Slump slides are relatively shallow surficial failures in levees which occur usually after a heavy rainfall with a long period of drying (Sills, 1983). Moisture retention and then the wet-dry cycle decrease soil suction and reduce soil shear strength which can lead to slump slide occurrence. Erosion in levees with cohesive soils may occur due to existence of cracks and/or hydraulic fractures caused by differential settlement during construction or operation, and/or low stresses near conduits or due to high level desiccation in the fill (Fell & Fry, 2013). Among different modes of failure in levees, seepage and underseepage are crucial factors for distress conditions. They can negatively affect slope stability by reducing effective stresses in the levee body and foundation soil (Bhowmik et al., 1994; Flor et al., 2010).

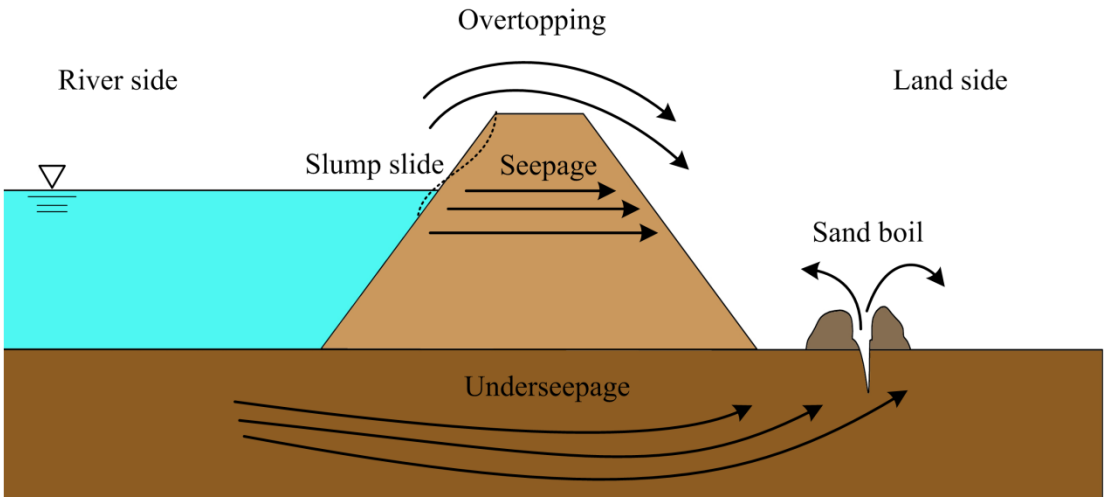

Figure 1 Conceptual levee failure mechanisms (after Bogardi and Mathe, 1968)

Significant attempts have been made in the last few years to enhance the knowledge of levee monitoring including the development of real-time in situ monitoring systems (e.g., Abdoun, et al., 2013), multi-scale monitoring techniques to provide early warning of distress and degradation (e.g., Zeghal et al., 2013), large scale remote-sensing based models (e.g., Aanstoos et al., 2012; Lv et al., 2013). A remote-sensing-based tool for early detection that can identify weak areas and impending failures could be an effective key to a more cost-effective monitoring system for levees (Lv et al., 2013).

An extensive research project for screening levees and detecting vulnerabilities by utilizing air-borne and space-borne synthetic aperture radar (SAR) systems was recently completed at Mississippi State University (Aanstoos et al., 2012). The main objectives of that project were developing a set of features and a number of automated supervised and unsupervised classifiers to apply to radar imagery in order to identify sections of levees vulnerable to failure. One unsupervised classification method tested was the algorithm proposed by Irving Reed and Xiaoli Yu (Reed and Yu, 1990), which is referred to as the Reed-Xiaoli Detector (RXD) algorithm. The RXD method is capable of detecting the presence of optical signal patterns and finds targets that have spectrally different signatures from their surroundings (Reed and Yu 1990, Chang and Chiang, 2002). After running the RXD-based classifier, sites that were recognized as vulnerable areas were visited to see if they would be of concern to levee managers. Site visits concluded that the classifier was able to correctly identify the location of the only active slump slide at the time of the radar image acquisition. However the classifier's output included some commission errors meaning that based on visual inspections, some areas detected by the classifier as anomalies were within apparently healthy areas of levee (i.e., areas where no

slope failures were observed). This type of error is referred to as a “false positive”. Site visits revealed that the vegetation type for many of these false positive points was different from that of the healthy areas (Aanstoos et al., 2012).

The main objective of this study is to examine these false positive points by comparing their soil properties with those of the active slide and healthy areas to find out if they have any similarity to either of these areas. To accomplish this task, imagery acquired by the NASA Uninhabited Aerial Vehicle Synthetic Aperture Radar (UAVSAR) was used along with in situ measurements of a variety of soil properties. Investigation of the vulnerability of false positive points can help levee managers to find high risk areas on levees before occurrence of major failures.

Study area

The Mississippi river is approximately 3,766 km long and its basin covers more than 3,224,000 km^2 that includes all or some parts of 31 states in the United States and two Canadian provinces. From the confluence of the Mississippi River with the Ohio River to the Gulf of Mexico where it disembogues is called Lower Mississippi River. The 1.7 km long study area focuses on the mainline levee system on the east side of Lower Mississippi River, north of Vicksburg, Mississippi (Fig. 2). The pertinent georeferenced layers used in the study and analyses have been masked by an approximately 40-meter wide buffer from the levee center line. This study area was selected to support the investigation of the use of remotely sensed data to analyze physical factors that may indicate slump slides on the river side of levee.

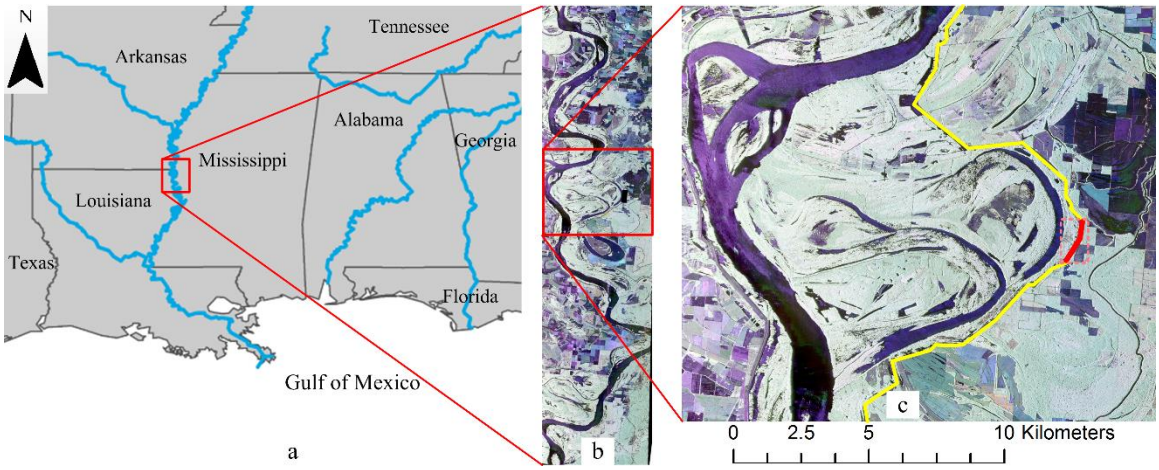

Figure 2 (a) Location of the study area in USA river map, (b) Polarimetric UAVSAR image of a part of Lower Mississippi river, (c) Levee system colored with yellow, and study area colored with red

Soil properties

An extensive set of in situ tests was conducted by C3 Consulting, LLC to collect various soil properties from the top 120 cm of soil over the entire study area. Information about soil texture, penetration resistance, hydraulic conductivity and moisture content were obtained. These soil properties were selected because of their relevance to earthen levee failure mechanisms.

The main sensor platform that was used to derive soil properties was a hydraulic push system (Fig. 3(a)). The system has a probe with different sensors that can be pushed into the ground with a push system and an onboard computer that runs the data acquisition and analysis software simultaneously. The geophysical probe is pushed into the ground to collect continuous data streams for tip resistance, moisture content and electrical conductivity. The miniaturized cone penetrometer which was used has a diameter of 3.175 cm, surface area of 10 cm^2 and cone angle of 60º (Fig. 3(b)). This

penetrometer was integrated with resistivity and moisture sensors which collected data on tip resistance, resistivity to electric current and soil compactness in increments of one centimeter to a depth of 120 cm. In order to supplement and verify the data obtained by the cone penetrometer and sensors and to obtain texture information, soil core sampling was performed to the depth of 120 cm at nearly 15 cm away from each penetration location. The whole sensor platform was used in conjunction with a real-time kinematic GPS unit to evaluate spatial variability of soil and topography across the study area.

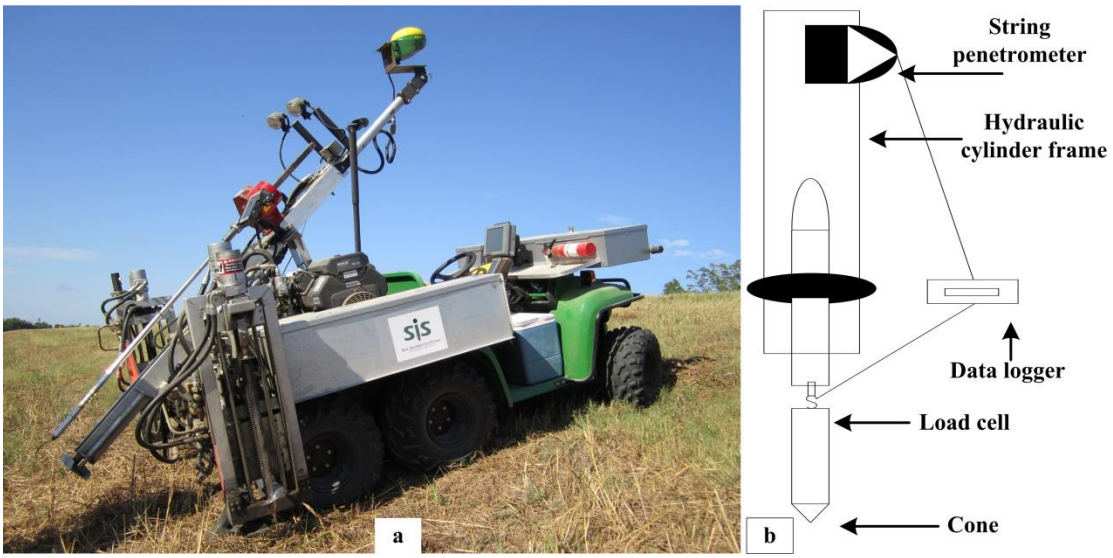

Figure 3 (a) Sensor platform in conjunction with an all-terrain vehicle-mounted. (b) Schematic view of cone penetrometer

The soil profile was broken into surface and subsurface layers. Omitting the top 7 cm of soil to ignore effects of anthropogenic activities, the surface layer was specified as extending from that level to the depth of 30 to 45 cm. The subsurface layer was specified from the bottom of the surface layer down to the depth of 120 cm. This depth interval

(top 120 cm) is suitable for the purpose of the current study which focuses on slump slides (i.e., relatively surficial failures). Moreover, L-band radar, which was used in this study, achieves one of the deepest penetration depths among radar bands but cannot penetrate the soil to more than a few cm depths. Any deeper signs of instability would not be directly observable by the radar, but they might have some correlation with surface anomalies. These correlations might be related to such phenomenon as small surface deformations, surface cracking and resulting drainage patterns, and common soil textures resulting from construction methods.

The data collected from the cone, sensors and soil corings were then integrated to map the soil properties and to generate raster layers showing the spatial distribution of each soil parameter of interest over the study area (Grunwald et al., 2001a). 67 data points in an area of about 26,400 m^2 were collected resulting in a penetrometer density of 1 per 394 m^2. At each point of measurement and in the vertical direction (i.e., along the depth), the geotechnical data was a continuous vertical transect from penetrometers and soil core samples. The average of measured values in each layer was selected as the representing soil property for that layer in the vertical direction. Then raster layers were created using the 2-D Kriging interpolation technique (Grunwald et al., 2001b). The spatial distribution of the measured data points was designed to uniformly cover different zones (healthy, slide, false positives) within the entire study area. It should be noted that using interpolated soil property maps may induce some uncertainties that can influence the results/conclusions. However, this is an inherent limitation associated with any analysis conducted using interpolated data. In the current study, using interpolated maps was inevitable considering the regional-scale of study and the raster-based nature of

analyses. The possible impact of using interpolated data was minimized by uniformly distributing measured points and by employing a robust interpolation technique. Soil mapping and the pertinent discussions are beyond the scope of this study and further details in this regard can be found in Grunwald et al. (2001b). The raster layers were suitable for performing regional scale analyses with ArcGIS. The pixel size of the soil properties raster layers was 1m × 1m.

The texture of the soil can be an indicator of vulnerability of the system to erosion (Fell & Fry, 2013). According to the USDA (United States Department of Agriculture) Textural Soil Classification (USDA, 1987), the soil in the study area consists of more than 55% clay and less than 25% sand. Clay and sand fraction distribution maps for the surface layer over the study area are shown in Fig. 4(a) and 4(b), respectively. Clay fraction for the surface layer varies between 56.1% and 64.6%.Sand fraction for the surface layer varies between 13.3% and 22.2%.

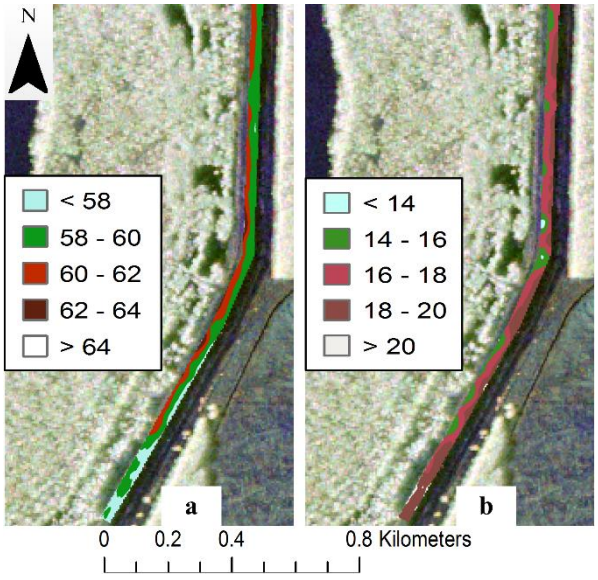

Figure 4 Soil texture for the surface layer. (a) Clay fraction (%) and (b) sand fraction (%).

The distribution of cone tip resistance over the study area is shown in Fig. 5(a). Cone index (CI) is the required force per unit area that is needed to push the cone penetrometer into a specific depth of soil (Grunwald et al., 2001a). Penetration resistance is the response signal from various soil properties such as texture, strength and compaction, moisture content, bulk density, etc. (Grunwald, 2006). Cone tip resistance for the surface layer varies between 917.5 kPa to 1,658.9 kPa.

Hydraulic conductivity is the amount of flow per unit area and is directly proportional to seepage velocity and is a key factor for seepage analysis. The distribution of hydraulic conductivity for the surface layer is shown in Fig. 5(b). Hydraulic conductivity for the surface layer varies between 0.18 cm/h to 0.22 cm/h.

When water soaks into soil structure, it lowers the strength by lessening cohesion (Cedergren, 1989); hence moisture content is an important parameter in stability of

levees. The distribution of moisture content for the surface layer over the study area is shown in Fig. 5(c). The moisture content in the surface layer varies between 32% and 46.3%.

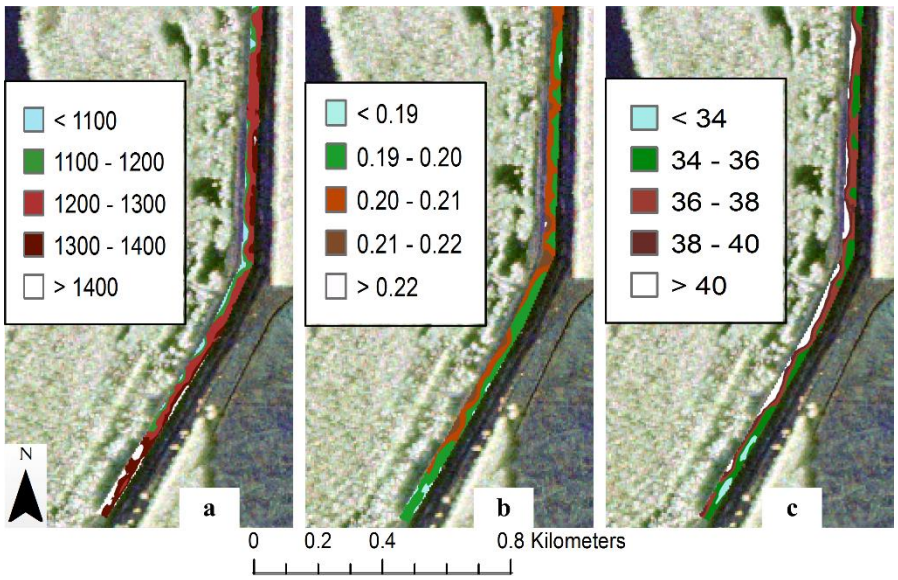

Figure 5 Soil properties for the surface layer. (a) Cone tip resistance (kPa), (b) hydraulic conductivity (cm/h), and (c) moisture content (%).

Similar raster layers were created for each soil parameter of interest for the subsurface layer but are not shown due to space limitation. However, statistics of the parameters for the subsurface layer are presented and discussed in the next sections.

Radar data, preprocessing and classification

In this project, a UAVSAR image acquired on January 25, 2010 was used. UAVSAR is a polarimetric L-band SAR. It was designed to obtain airborne repeat track SAR data for differential interferometric measurements (Rosen 2006). Providing spatially continuous data suitable for ground surface feature extraction in digital format, and

covering large areas with low costs are the main advantages of interferometric SAR in comparison to GPS surveying and photogrammetric methods (e.g., Colesanti and Wasowski 2006).

The radar is fully polarimetric, with a range bandwidth of 80 MHz and 1.8 m resolution. To acquire the radar imagery for this study, the flight was flown in a racetrack pattern looking towards the river from opposite directions to achieve a range of local incidence angles along the levees from which we could choose the best for our purposes. Although the raw ground sample distance is 1.6 by 0.6 m, we used multi-look 5 by 7 m data to minimize speckle effects. The radar data were already processed with a multi-look-based speckle reduction method by JPL (Aanstoos et al. 2012). The incidence angle of the radar beam varied across the image swath from 25 to 60 degrees. The net local incidence angle was further modified by the slope and orientation of the levee. The preprocessing of the radar data included adjustments for terrain based on an elevation map. However, variations in incidence angle can affect how backscatter magnitude depends on surface roughness. To minimize this effect for this study, the study area was limited to a segment of levee with a constant orientation and slope. Table 1 summarizes the key UAVSAR parameters.

Table 1 Key UAVSAR instrument parameters

Parameter	Value
Frequency	L-band
Bandwidth	80 MHZ
Azimuth steering	> ± 20°
Range Resolution	1.8 m
Polarization	Full Quad-Polarization
Raw ADC Bits	12 baseline
Waveform	Nominal Chirp/Arbitrary Waveform
Antenna Dimensions	0.5 m range/1.5 azimuth
Power	> 2.0 kW
Polarization Isolation	<-20 dB

Image classification is an important step in image analysis. However, before this step, feature extraction must be implemented. The map classification procedure is illustrated in Fig. 6. Features are statistical characteristics of image data. In the study area, surface roughness is a property that can be used to distinguish slump slide locations. Surface roughness is the terrain property that most strongly influences the strength of radar backscatter (Jensen 2007). Therefore a feature that correlates well to the surface roughness was applied to the classifier: the low frequency sub-bands of the discrete wavelet transform.

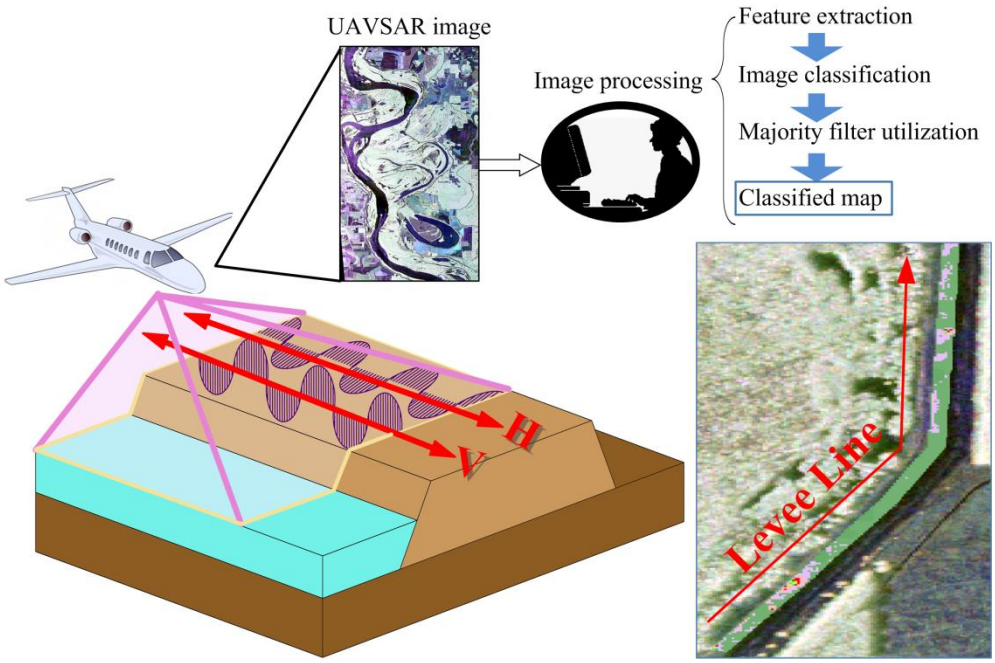

Figure 6 The process of map classification from UAVSAR imagery in the study area.

Image classification is the process of assigning classes to component pixels of an image in a way that pixels within a class are more similar than pixels in other classes (Campbell, 2007). Figure 7(a) shows the UAVSAR image for the study area before applying the classifier. Based on the characteristics of the image over the study area, the RXD algorithm was used for classification. It is a training-free unsupervised classifier and is commonly used as a benchmark for anomaly detection purposes. It is fast and has been successfully utilized to detect anomalies of multispectral images (e.g., Ashton and Schaum, 1998, Stellman et al., 2000). The algorithm calculates the Mahalanobis distance from the test pixels to the mean of the background pixels. If L is the number of features, r is a L × 1-column pixel vector of the image, then the RXD method implements a filter specified by

$$\delta_{RXD}(r) = (r - \mu)^T K_{L\times L}^{-1} (r - \mu) \quad (1)$$

where μ is the global sample mean and $K_{L\times L}$ is the sample covariance matrix of the image. Using the backscatter magnitudes of the horizontal and vertical co-polarized channels (HH and VV) from the radar data along with the discrete wavelet transform resulted in 8 features in the current study. For computation purposes, we used a window size of 4 × 4 pixels, and computed the wavelet coefficients for both HH and VV channels. The output generated by RXD is a grayscale image. The larger the gray values of the pixels, the more anomalous the pixels would be. For visualization purposes, ranges of values of the output are often color-coded.

Based on the available field data and field visits, the location of the slide was known before the classifier detected it as an anomaly. Therefore the geometry of the slide was drawn using ERDAS Imagine (software with raster graphics editing capabilities) based on the data collected from field visits as well as several aerial photos from the study area. The location of the slide that was detected by the classifier is shown in Fig. 7(b) and is at the southern end of the study area. The slide dimensions were provided by the Mississippi Levee Board. It was about 61 m long and 2.43 m deep. The depth was measured from the height of the scarp/wall from the top of the unbroken land (also called crown) down to the slide debris. The width varied in length from less than 7 m to 36 m.

After running the classifier, it was concluded that the classifier was able to correctly identify the slide location since the pixels in that area had higher values of normalized Mahalanobis distance. A histogram for the normalized Mahalanobis values in the slide region was plotted to see their distribution in this area. Quantitative assessment of soil properties for the different segments identified by the anomaly

detection algorithm requires applying a threshold to the pixel values of the classifier's output. Various threshold values were examined with the goal of maximizing the percentage of true positives (i.e., slide pixels detected) and minimizing the percentage of false positives. A threshold of 0.002 was chosen which resulted in over 90% true positives and less than 20% false positives. RXD is an unsupervised classifier resulting in grayscale images and the detection of anomalies is usually carried out through visual inspection (Chang and Chiang, 2002). The purpose of selecting a threshold in this study was to segment the study area for post-analysis that could inform the design of a more robust classifier in the future. The use of all of the "ground truth" data (in this case the pixels of the only active slide in the study area) to guide the selection of a threshold should not be confused with the testing of a classifier for accuracy – for such purposes it would not be statistically sound to use the same data for "training" and "testing". We make no quantitative statement about the accuracy of the RXD method as a slide classifier. Based on the chosen threshold, regions with values less than the threshold were called "healthy area" and the regions with values greater than the threshold were called "anomalous pixels" (Dabbiru et al., 2012). As shown in Fig. 7(b), among the anomalous pixels, the classifier's output included some false positive points which means that some detected targets classified as anomalous pixels actually appeared healthy in site visits and no visible slide was noticed in that time within those areas.

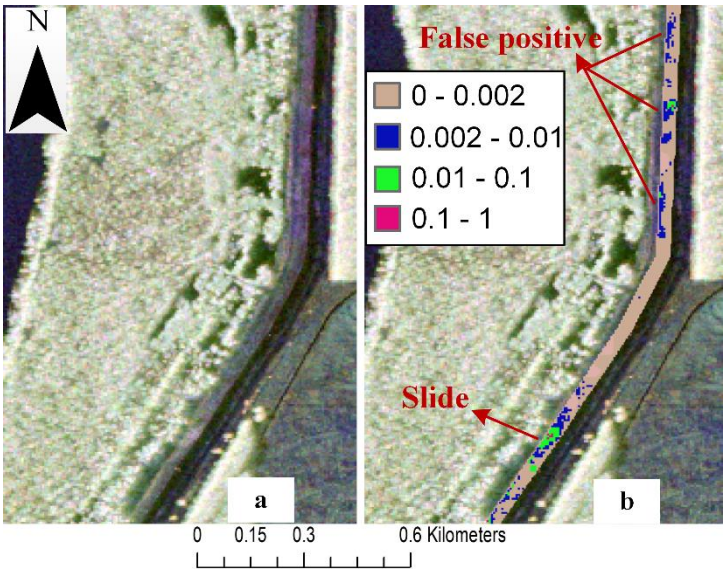

Figure 7 (a) UAVSAR image over lower part of study area. (b) Classified map with RX anomaly detector showing normalized Mahalanobis distances for the study area.

What brought our attention to these false positive points were two facts. First, as noted earlier, site visits showed that the vegetation type for many of these false positive points was different from the grass that was covering most of the healthy areas (Aanstoos et al., 2012). Second, after the time of the UAVSAR flight, cracks appeared and vegetation became stressed in the location of some of these false positive points. Therefore we decided to analyze different soil properties of these false positive points and compare them with that of the slide and healthy areas to see if there may be an increased potential for false positives to slide

The lack of ability for discriminating the detected targets from another is known as a disadvantage for anomaly detectors (e.g., Chang and Chiang, 2002). This disadvantage of anomaly detection is mitigated in this study by the fact that the targets are on man-made levees which are designed to be quite homogeneous. Therefore, any

significant anomalies have a high likelihood of being at least areas of interest to levee inspectors.

Comparison of in situ data for false positive points, slide, and healthy areas

Most remote sensing land use classification studies are based on pixel information (Castillejo-González et al. 2009). Therefore in order to investigate the vulnerability of the false positive points to future slump slides, per-pixel statistical analyses were included when examining the distribution of five relevant soil parameters and comparing these from the slide and healthy areas. The size of the pixels in the classifier's output was 5.5 m × 5.5 m. In total, the classifier's output included 1,633 pixels of which 67 pixels corresponded to the slide area (true positives), and 317 pixels corresponded to the false positive pixels.

The first method of analysis was performed by pixel-based comparison of soil data for all false positive pixels with that for all pixels of the slide and healthy areas. However, when the spatial resolution increases, the intraclass spectral variability increases as well and finally, the classification performance decreases (Castillejo-González et al., 2009). So a second method of analysis, object-based comparison, was also used in which regions containing a high density of false positives were analyzed. The two zones shown in Fig. 8(b) labeled as FP1 and FP2 were selected for this object-based method. They both have similar shapes and geometry to the slide area. Our field visits and the report of previous slide occurrences provided by the Mississippi Levee Board revealed that FP2 is a repaired slide. This object-based analysis was conducted to specifically compare soil properties of these dense false positive zones with the slide and

healthy areas. The results from each analysis method are presented and discussed separately in the following sections.

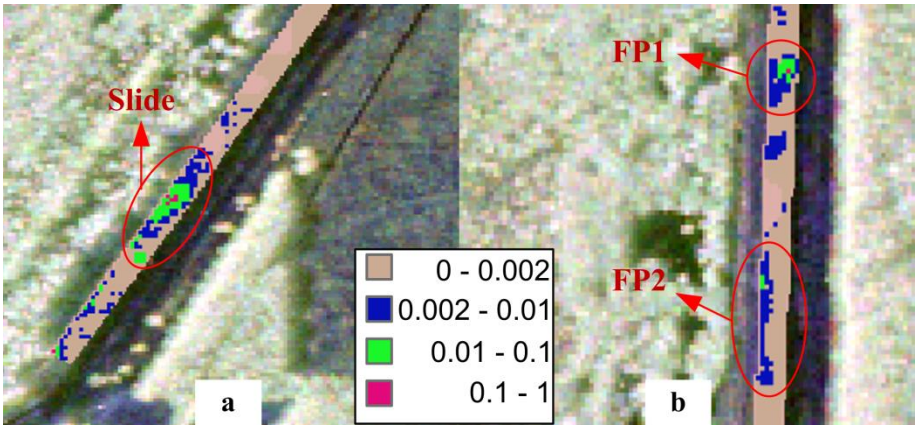

Figure 8 (a) Location of the slide and (b) dense false positive zones of FP1 and FP2 (legend shows normalized Mahalanobis distances for the study area).

Method 1: Pixel-based comparison of false positives, healthy and slide areas

Prior to compiling statistics using the pixel-based method (Method 1), in order to improve the accuracy of the classified output and to decrease the amount of isolated false positive pixels, a majority filter was applied to the classified image in ArcGIS. Majority filters replace cells of a raster based on the majority of their contiguous neighboring cells. Four direct (orthogonal) neighbors to the present cell were used in the kernel of the majority filter.

Method 1, surface layer

The histogram distributions and statistics summary of the analyzed soil parameters are shown in Fig. 9 for the surface layer. The clay fraction ranges between 57.4 and 60.8%, 56.1 and 63.5%, and 56.6 and 64.6% in the three areas with means of

59.6%, 59.3%, and 60% for the slide, healthy, and false positives, respectively. This trend shows that in the study area, the healthy areas have lower clay fraction compared to the slide and false positives (Fig. 9(a)). The sand fraction varies from 14.3 to 18.7%, 13.3 to 21.2%, and 13.3 to 22.2% for slide, healthy and false positives, respectively. More than 40% of the three areas have sand fraction of 16%-18%. The averages are 16.2%, 17.6% and 16.9% for the slide, healthy, and false positives, respectively (Fig. 9(b)).

The cone tip resistance for the surface layer ranges between 1,107.5 and 1,521.9, 973.5 and 1,618.9, 917.5 and 1,658.9 kPa, with means of 1,248.6, 1,260.3 and 1,236.2 kPa for the slide, healthy areas, and false positives, respectively. There can be seen a similar positively skewed distribution in the false positives and slide area while it is a log normal distribution for the healthy areas. These trends show that the false positives have lower tip resistance than the healthy areas and even slide area ((Fig. 9(c)). As shown in Fig. 9(d), the moisture content for the surface layer varies from 33.7 to 39.5%, 32 to 44.8%, and 32.3 to 46.3% in slide, healthy and false positive areas respectively. The slide area has moisture content average of 36.6%. The false positives have a unimodal distribution of moisture content with a mean of 38.3% in this range, while the healthy area has almost a log normal distribution with a mean of 37.3%.

Fig. 9(e) shows the hydraulic conductivity histograms which range between 0.19 and 0.22 cm/h for slide area, 0.18 and 0.22 cm/h for healthy and false positive areas. According to the histogram shown in Fig. 9(e), the healthy area has a positively skewed distribution with a mean value of 0.20 cm/h and a 50% concentration in the range 0.19-0.20 cm/h. Both the false positives and slide area have a log normal distribution with means of 0.20 cm/h and 0.21 cm/h, respectively. More than 80% of soil of these two

areas has a hydraulic conductivity falling in the range of 0.20-0.22 cm/h. This is consistent with the fact that the false positives and slide area have higher amount of clay fraction than the healthy area.

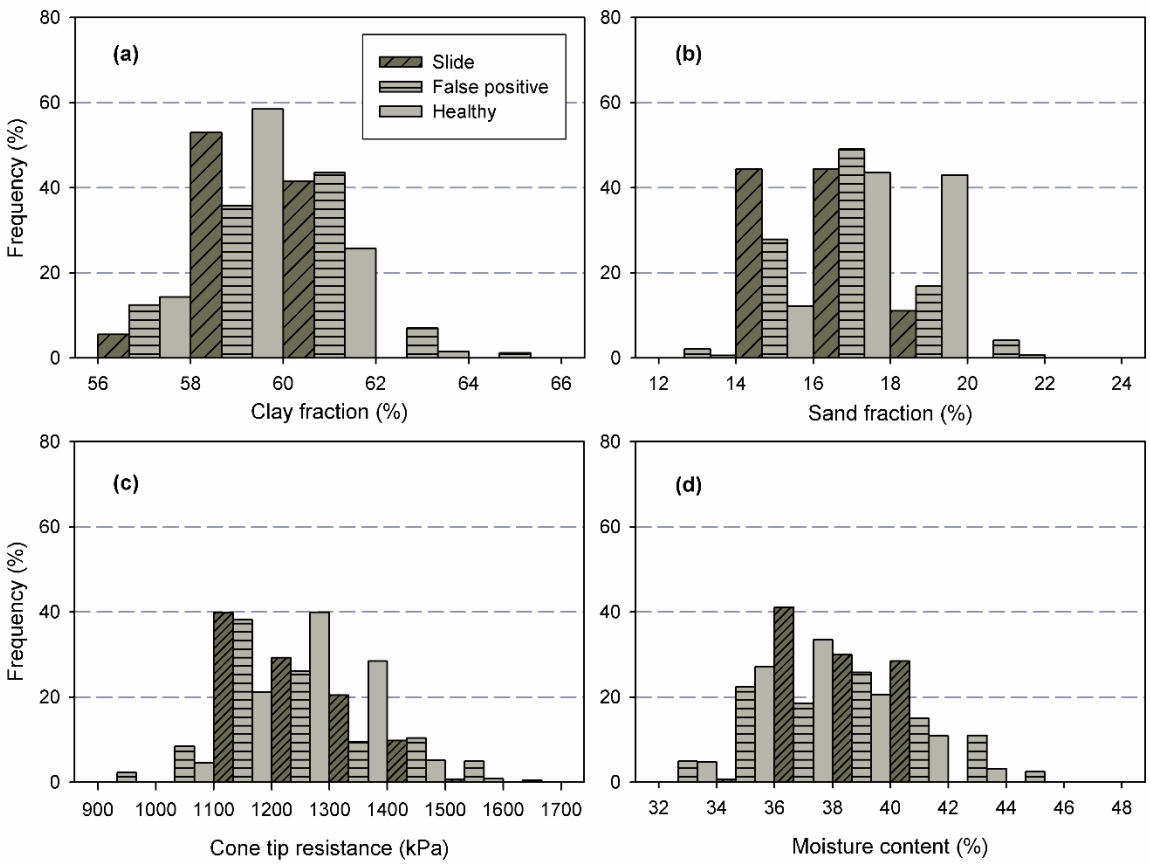

Statistics summary

Parameter		Slide	Healthy	F.P.
Clay (%)	Ave.	59.6	59.3	60.0
	SD	0.85	1.2	1.6
Sand (%)	Ave.	16.2	17.6	16.9
	SD	1.2	1.3	1.6
q_c (kPa)	Ave.	1,248.6	1,260.3	1,236.2
	SD	100.5	93.6	134.8
ω (%)	Ave.	36.6	37.3	38.3
	SD	1.6	2.3	2.9
K (cm/h)	Ave.	0.21	0.2	0.2
	SD	0.005	0.006	0.007

Note: q_c: Cone tip resistance, K: Hydraulic conductivity
ω: Moisture content, SD: Standard deviation.

Figure 9 Histogram distribution of (a) clay fraction, (b) sand fraction, (c) cone tip resistance, (d) moisture content, and (e) hydraulic conductivity of the surface layer using Method 1.

Method 1, subsurface layer

In the subsurface layer, unlike the surface layer, the distributions of soil properties of the false positives and healthy areas are more similar to each other than to those of the slide area. Fig. 10 shows the histograms and statistics summary of the in-situ soil properties for the slide, healthy areas and false positives in the subsurface layer. As shown in Fig. 10(a), the clay fraction for the subsurface layer varies from 56 to 63.3% in the three areas. Almost 90% of pixels from the slide area have clay fraction in the range of 58-60 % with a mean of 58.5%, while both the healthy and false positive areas have normal distribution for the clay fraction with means of 59.2 and 58.9%, respectively. The sand fraction values vary from 15.9 to 25.2% in the three areas (Fig. 10(b)). There can be seen a positively skewed distribution in the slide area with a mean of 18.5%, while it is a log normal distribution for the false positives and healthy areas with means of 20.7 and 21.7%, respectively. More than 80% of pixels in the healthy and false positive areas have sand fraction of 20 to 24% while this number varies from 16 to 20% for the slide area.

As shown in Fig. 10(c), cone tip resistance for the subsurface layer ranges between 683 to 1,255.5 kPa. More than 70% of the slide area have tip resistance of 1,000-1,100 kPa with a mean of 1,063.8 kPa. The healthy and false positive areas have a log normal distribution with a concentration of more than 40% in the range of 900-1,000 kPa and 1,000-1,100 kPa, respectively. The mean of cone tip resistance data in the subsurface layer is 978.5 kPa for the healthy areas and 1,021.5 kPa for the false positives. According to the histogram shown in Fig. 10(d), almost 80% of the soil in all the three areas has moisture of 56-58%. The means of moisture content for the subsurface layer is 57.4, 56.8

and 56.9% for the slide, healthy and false positives, respectively. This shows that the false positives and healthy areas have almost similar moisture content values.

As illustrated in Fig. 10(e), the hydraulic conductivity values in the subsurface layer vary from 0.17 to 0.21 cm/h in the three areas. Almost 80% of the slide area pixels have hydraulic conductivity of 0.19-0.21 cm/h with a mean of 0.20 cm/h. More than half of the false positives and the healthy areas have hydraulic conductivity in the range of 0.18-0.19 cm/h with means of 0.19 cm/h and 0.18 cm/h, respectively. This trend shows a high similarity between the false positives and the healthy areas.

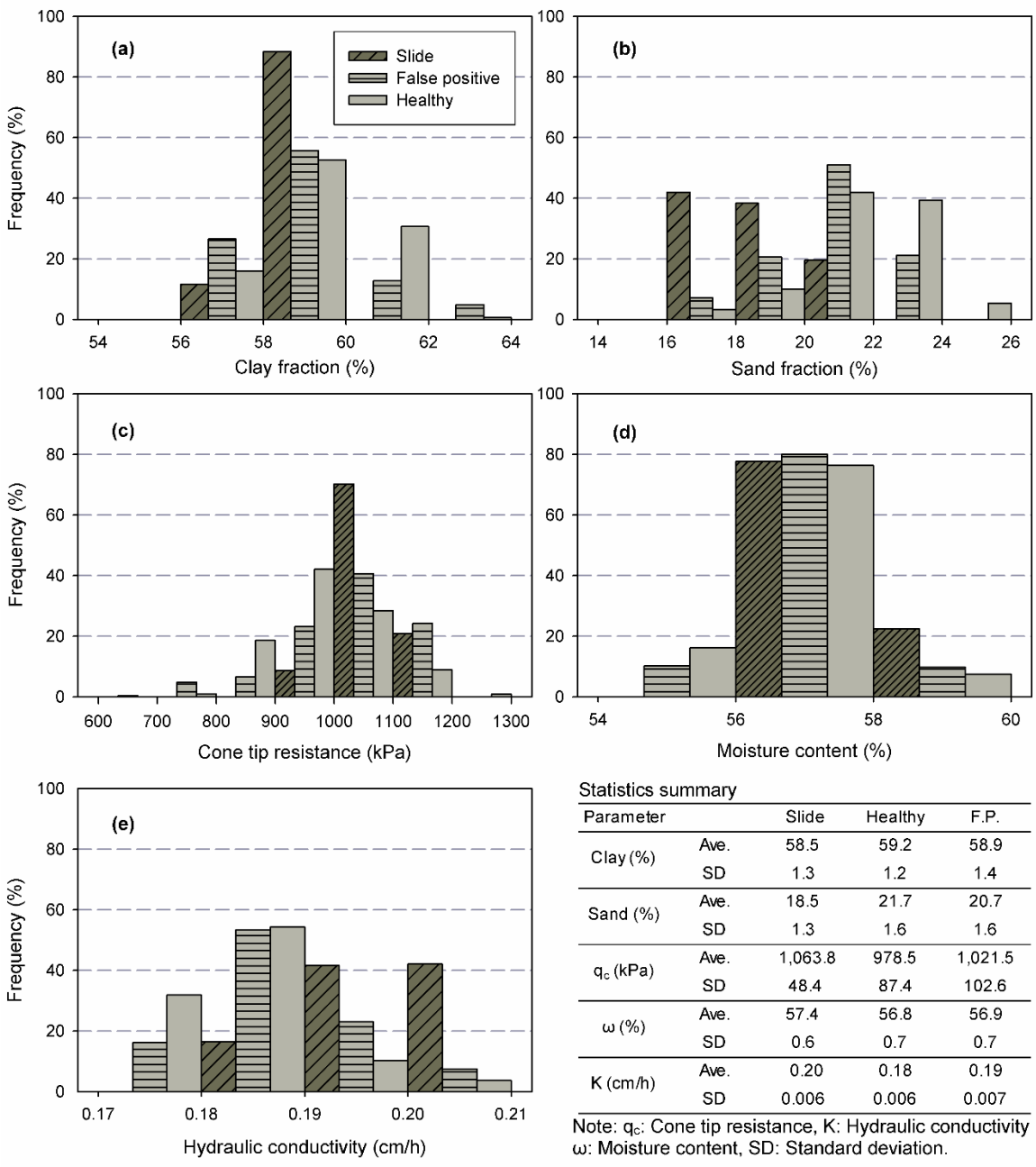

Statistics summary

Parameter		Slide	Healthy	F.P.
Clay (%)	Ave.	58.5	59.2	58.9
	SD	1.3	1.2	1.4
Sand (%)	Ave.	18.5	21.7	20.7
	SD	1.3	1.6	1.6
q_c (kPa)	Ave.	1,063.8	978.5	1,021.5
	SD	48.4	87.4	102.6
ω (%)	Ave.	57.4	56.8	56.9
	SD	0.6	0.7	0.7
K (cm/h)	Ave.	0.20	0.18	0.19
	SD	0.006	0.006	0.007

Note: q_c: Cone tip resistance, K: Hydraulic conductivity
ω: Moisture content, SD: Standard deviation.

Figure 10 Histogram distribution of (a) clay fraction, (b) sand fraction, (c) cone tip resistance, (d) moisture content, and (e) hydraulic conductivity for the subsurface layer using Method 1.

Method 2: Object-based comparison of false positives, healthy and slide areas

For performing the object-based analysis, two zones of dense false positives, labeled as FP1 and FP2 in Fig. 8(b), were compared with the slide and healthy areas. As can be seen in Fig. 8(b), FP1 is located in the northern part of the study area, and FP2 is almost in the middle of the study area, about 640 meters away from the slide.

Method 2, surface layer

Fig. 11 shows the histograms distribution and statistics summary of the in-situ soil properties for the slide, healthy areas, FP1, and FP2 in the surface layer. In the surface layer, the clay fraction distribution ranges from 56.1 to 64.6% in the four areas (Fig. 11(a)). More than half of the pixels in the slide, healthy areas and FP1 have a clay fraction of 58-60%, while this range is higher and is 60-62% for FP2. The slide area has a positively skewed distribution with min of 57.4 and max of 60.8%. The healthy area has a normal distribution with a min of 56.1 and max of 63.5%. FP1 and FP2 have positively skewed distributions with min of 58.2 and 59.6%, and max of 62.1% and 64.6%, respectively. This trend shows higher amount of clay fraction in the slide, FP1 and FP2 compared to the healthy area. As shown in Fig. 11(b), the sand distribution ranges from 13.3 to 21.2% in the four areas. The slide area has sand fraction with min and max values of 14.3 and 18.7%, an average of 16.2%. Sand fraction in the healthy area has nearly a normal distribution with a mean of 17.6%. FP1 and FP2 have negatively skewed distribution with means of 16.8 and 15.8%, min values of 14.8 and 13.3%, and max values of 18.1 and 17.3%, respectively. This trend demonstrates how the slide, FP1 and FP2 have significantly lower sand fraction than the healthy area.

Cone tip resistance varies from 917.5 to 1,618.9 kPa in the four areas. Tip resistance for the slide area has a positively skewed distribution with a mean of 1,248.6, min of 1107.5 and max of 1,521.9 kPa. The healthy area has a normal distribution with a mean of 1,260.3, min of 973.5 and max of 1,618.9 kPa. Tip resistance mostly varies between 1,100 to 1,300 kPa for FP1. It has a mean of 1,201.3, min of 1070.6 and max of 1,313 kPa. There is a negatively skewed distribution in FP2, with a mean of 1,114.4, min of 917.5 and max of 1,252.4 kPa. These numbers show how significantly low the tip resistance is in the slide area and in FP1 and FP2 compared to the healthy area (Fig. 11(c)). Fig. 11(d) shows the moisture content distribution ranging between 32 and 44.8% in the four areas. The slide has almost a unimodal distribution in the range 34 to 40% with a mean of 36.6%, min of 33.7%, and max of 39.5%, while the healthy areas have a normal distribution with a mean of 37.3%, min value of 32%, and max value of 44.8%. The moisture content distribution in FP1 is very similar to that in the slide area distribution with a mean of 36.7%, min of 34.3%, and max of 39.8%. FP2 has a normal distribution with a mean of 40.9%, min of 36.7%, and max of 44.6% which are even higher than that of the slide area. The overall trend shown in Fig. 11(d) indicates that the distribution of moisture content in FP1 and the slide area are significantly similar to each other, and interestingly, FP2 has much higher moisture content than any other classified area.

As shown in Fig. 11(e), hydraulic conductivity varies between 0.18 and 0.22 cm/h in the four areas. More than 70% of FP1 and FP2 have hydraulic conductivity of 0.20-0.21 cm/h where more than half of the slide area falls within that range too. The means for FP1, FP2 and the slide are 0.20, 0.21 and 0.21 cm/h, respectively. Hydraulic

conductivity has a positively skewed distribution in the healthy areas with a mean of 0.20 cm/h, min of 0.18 cm/h, and max of 0.22 cm/h. The overall trend observed in the distributions of hydraulic conductivity in the two dense false positive zones shows the values are as high as that in the slide area.

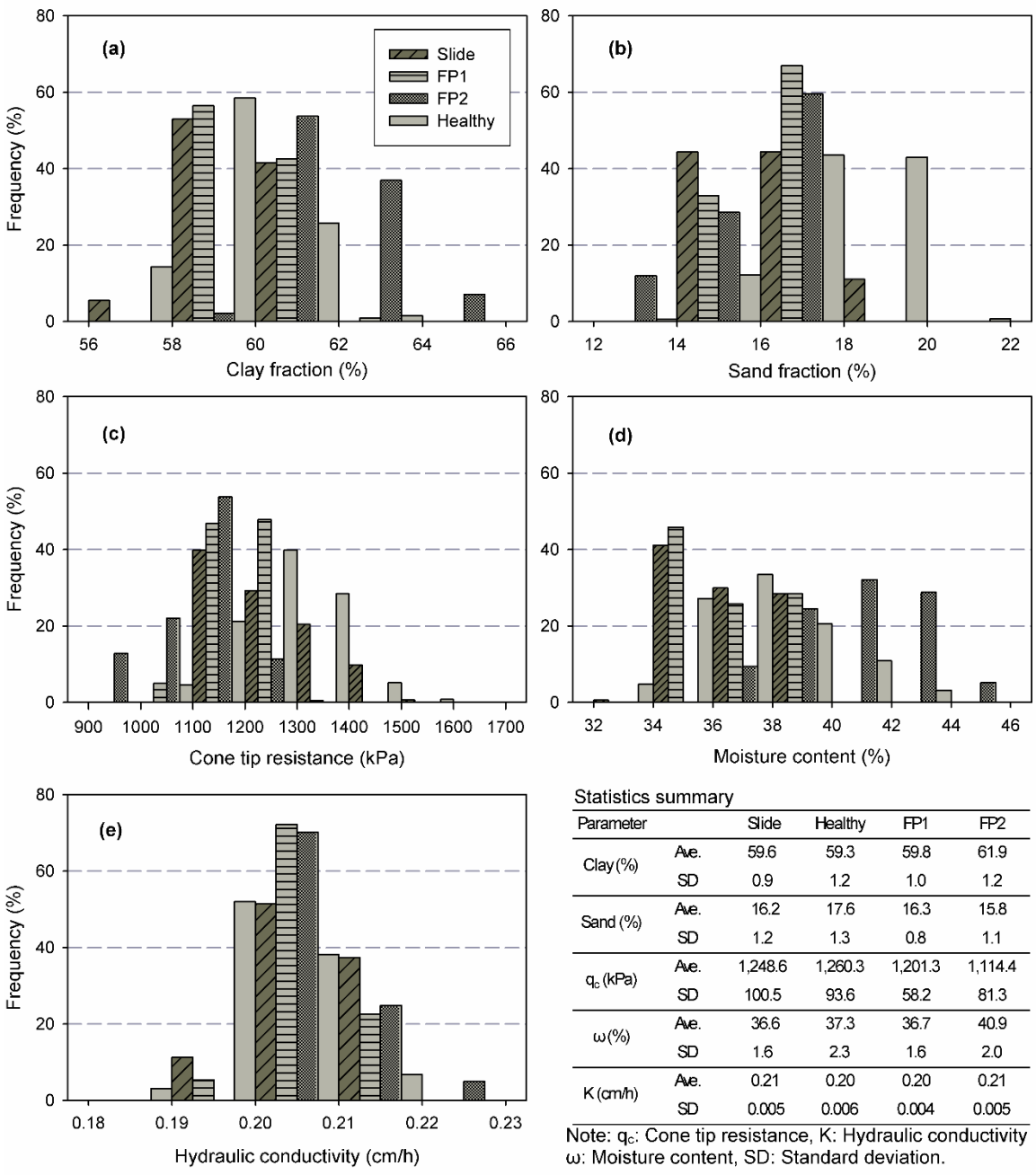

Statistics summary

Parameter		Slide	Healthy	FP1	FP2
Clay (%)	Ave.	59.6	59.3	59.8	61.9
	SD	0.9	1.2	1.0	1.2
Sand (%)	Ave.	16.2	17.6	16.3	15.8
	SD	1.2	1.3	0.8	1.1
q_c (kPa)	Ave.	1,248.6	1,260.3	1,201.3	1,114.4
	SD	100.5	93.6	58.2	81.3
ω (%)	Ave.	36.6	37.3	36.7	40.9
	SD	1.6	2.3	1.6	2.0
K (cm/h)	Ave.	0.21	0.20	0.20	0.21
	SD	0.005	0.006	0.004	0.005

Note: q_c: Cone tip resistance, K: Hydraulic conductivity
ω: Moisture content, SD: Standard deviation.

Figure 11 Histogram distribution of (a) clay fraction, (b) sand fraction, (c) cone tip resistance, (d) moisture content, and (e) hydraulic conductivity for the surface layer for Method 2.

Method 2, subsurface layer

The results of analyses from Method 2 for the subsurface layer are presented in Fig. 12. In the subsurface layer, the clay fraction distribution varies between 56 and 63.3% in the four areas (Fig. 12(a)). Almost 90% of the slide area and FP1 have clay fraction of 58-60%. FP2 has a normal distribution with a mean of 61%, min of 59% and max of 63.3%. The healthy area also has a normal distribution with a mean of 59.2%, min of 56% and max of 62.7%. There cannot be seen a specific relationship in these trends. As shown in Fig. 12(b), the sand fraction distribution varies between 16.1 and 25.2% in the four areas. The slide area has a positively skewed distribution with a mean of 18.5%, min of 16.4%, and max of 20.7%. Almost 80% of the healthy area pixels have a sand fraction of 20-24%. The mean, min, and max in this area are 21.7, 16.1 and 25.2%. FP1 has a unimodal distribution with a mean of 20.9%, min of 19.1%, and max of 23.8%. FP2 has a negatively skewed distribution with a mean of 22%, min of 19.6%, and max of 23.3%. The total trend shows that the slide and FP1 have lower fraction of sand while the healthy area and FP2 have larger sand fraction. No specific relationship between the slide area and the dense false positives zones can be detected.

The distribution of cone tip resistance for the subsurface layer is shown in Fig. 12(c). Cone tip resistance changes from 683 to 1,255.5 kPa in the four areas. More than 70% of the slide area pixels have a tip resistance of 1,100-1,200 kPa. The mean, min, and max values for the tip resistance distribution in the slide area are 1,063.8, 905.5, and 1,187.4 kPa, respectively. The healthy areas have a normal distribution for tip resistance with a mean of 978.5 kPa, min of 729.5 kPa, and max of 1,255.5 kPa. Almost 90% of FP1 pixels have a tip resistance of 1,000-1,200 kPa. The mean is 1,082.9 kPa, min and

max values are 903.6 and 1,150.5 kPa, respectively. FP2 has a bimodal distribution with a mean of 880.8 kPa, min of 683 kPa, and max of 1,071.9 kPa. According to the histograms, the tip resistance distribution for both the slide and FP1 is higher than that for the healthy area. However FP2 has the lowest tip resistance among the other classified areas. Moisture content in almost 80% of the four areas is in the range of 56-58% with means of 57.4, 56.8, 56.8 and 57.1% in the slide, healthy, FP1 and FP2, respectively (Fig. 12(d)).

Hydraulic conductivity ranges between 0.17 and 0.21 cm/h in the four areas (Fig. 12(e)). The hydraulic conductivity for more than 80% of the slide area varies in the range of 0.19-0.21 cm/h while the healthy area has a positively skewed distribution with a mean of 0.18 cm/h, min value of 0.17 cm/h, and max value of 0.21 cm/h. Almost 80% of FP1 varies in the range 0.18-0.20 cm/h with a mean of 0.19 cm/h. The distribution of hydraulic conductivity of FP2 ranges between 0.17 and 0.19 cm/h with a mean of 0.18 cm/h. The trend shows that the slide area has higher hydraulic conductivity in comparison to the other areas.

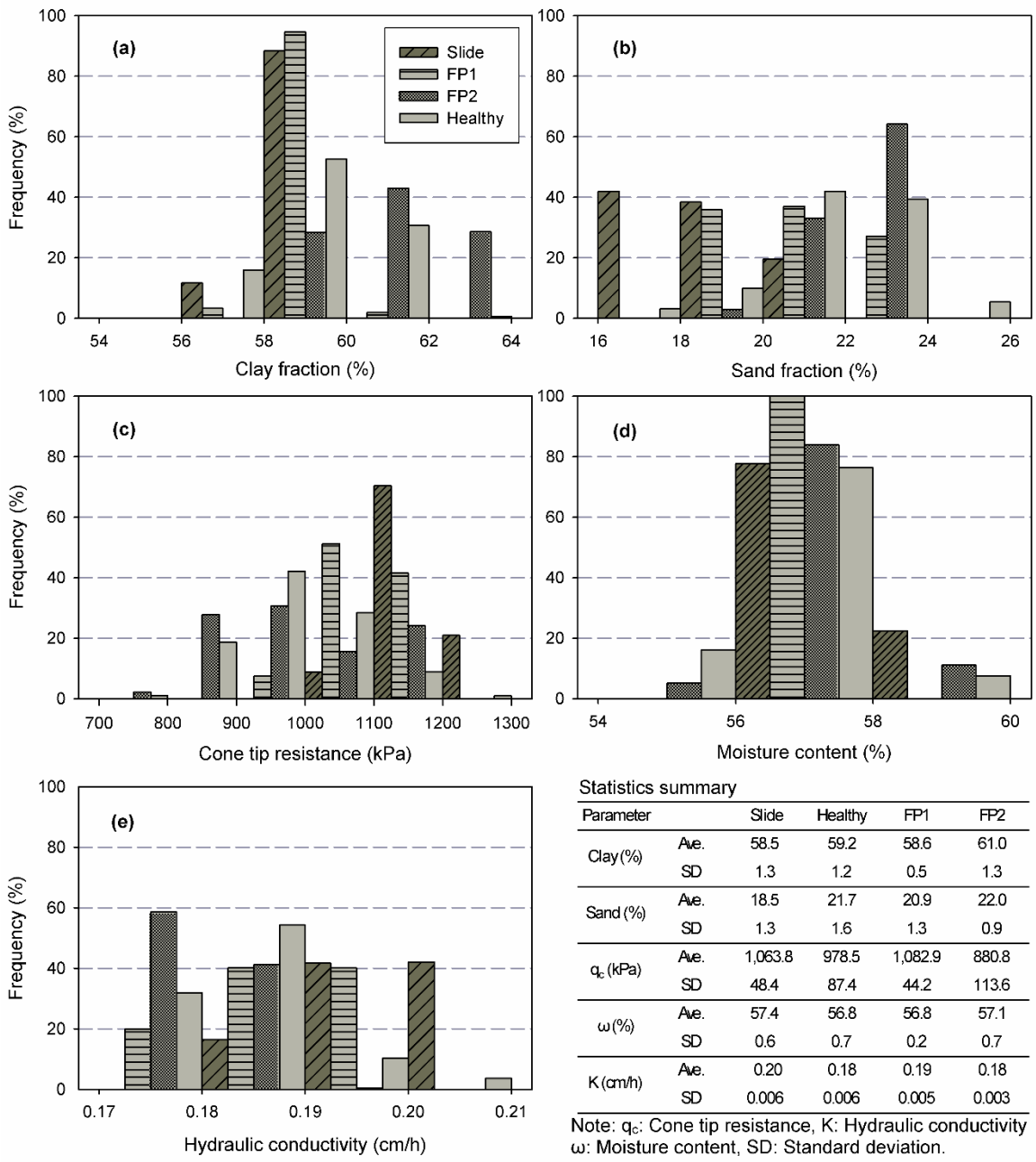

Statistics summary

Parameter		Slide	Healthy	FP1	FP2
Clay (%)	Ave.	58.5	59.2	58.6	61.0
	SD	1.3	1.2	0.5	1.3
Sand (%)	Ave.	18.5	21.7	20.9	22.0
	SD	1.3	1.6	1.3	0.9
q_c (kPa)	Ave.	1,063.8	978.5	1,082.9	880.8
	SD	48.4	87.4	44.2	113.6
ω (%)	Ave.	57.4	56.8	56.8	57.1
	SD	0.6	0.7	0.2	0.7
K (cm/h)	Ave.	0.20	0.18	0.19	0.18
	SD	0.006	0.006	0.005	0.003

Note: q_c: Cone tip resistance, K: Hydraulic conductivity
ω: Moisture content, SD: Standard deviation.

Figure 12 Histogram distribution of (a) clay fraction, (b) sand fraction, (c) cone tip resistance, (d) moisture content, and (e) hydraulic conductivity for the subsurface layer for Method 2.

Discussion

The overall trend observed from the two methods leads to the conclusion that in the surface layer, the false positives and the slide area were following similar trends in the distribution of different relevant soil measurements. In contrast to the surface layer, in the subsurface layer the false positives and the healthy areas were following similar trends, and sometimes the three areas had similar soil distribution. As UAVSAR is capable of penetrating soil to a few centimeters depth, the most accurate results for classification were derived at the surface layer. Therefore distinct trends of soil measurement distribution were mostly found in the surface layer, while no specific trends were seen in the deep subsurface layer. As mentioned in the previous sections, the UAVSAR image acquired from January 25, 2010 was used in this study. It should be noted that a slide had occurred at the location of FP2 in October of 2009 which was repaired in November of the same year. However, during our field visits in 2011 linear cracks perpendicular to the levee slope were discovered in that area. As shown in Fig. 13, grass growing in this location was also stressed and sparse compared to the surrounding areas. It was identified as an area of weakness based on these evidences. One possible hypothesis to explain the occurrence of cracks could be that it is an early sign of reactivation of the repaired slide.

Figure 13 Sparse grass (left) and cracks (right) in FP2 observed after the UAVSAR image acquired for this study.

The high rate of false positives observed in the classified results is with respect to the original definition of a true positive- a visibly detectable slide. The “true positive” points (i.e., active slide) used in the analysis were simply defined according to field visits. However, an earthen levee can suffer damages which can't be easily recognized in the field. For example, small deformations which might precede a visible slide could not be detected by means of a simple inspection. Sometimes they do not generate visible cracks previous to failure or are filled by sediments or eroded by rainfall. Evidence of these pre-slide displacements, which can cause surface geomorphological changes detectable by the radar-based technique, may be present in the soil properties sampled in this study. While no obvious sign of a slide is noticeable on the ground surface, internal erosion and damage might be progressing from the subsurface to surface in these false positive points which make them vulnerable for near future slides. That is, we investigated the hypothesis that the areas classified as false positive might actually be unstable although the field inspection would not have allowed recognizing the area as such. A major goal of

this post-analysis study was to see if we can expand the target classification to include non-visible areas of slope instability that might be detectable with in situ soil property measurements. If this turns out to be verified in larger studies it would be of great benefit to levee managers by providing a remote-sensing based way to screen large areas for more targeted intense inspections.

CHAPTER III

EFFECTS OF RAINFALL, GEOMETRICAL AND GEOMORPHOLOGICAL VARIABLES ON VULNERABILITY OF THE LOWER MISSISSIPPI RIVER LEVEE SYSTEM TO SLUMP SLIDES

Introduction

Levees are located in nearly 22% of the United States (U.S.) counties where half of the population of the country resides (CRS, 2011). Levees and other structures such as embankments and dams are becoming of major importance due to recent climate trends such as sea level rising and more rough weather events (i.e., floods, hurricanes and heavy rainfalls) (Bennett et al., 2014). The 2005 Hurricane Katrina is a well-known example of how the increasing frequency of extreme events due to climate change could have resulted in catastrophic failures in levees (Dupray et al., 2010). Record of the previous events shows that levee failures can lead to catastrophic damages to economy, infrastructure and population in the affected areas.

Monitoring levees is usually performed by inspectors walking on the levees looking for qualitative indications reflecting a change or coherence loss in the body of the levee (Dupray et al., 2010). However, the visual inspection method is expensive, time consuming, and impractical during emergencies. Therefore, the need for improving the reliability of levees as well as advancing monitoring techniques is inevitable. Design, construction and maintenance of levees should assure the integrity of levees against

different failure modes with satisfactory margin of safety during the life span of structure. While different design methods have been used for the U.S. levee systems, geological studies in the area of interest is a mandatory step for any design procedure. According to the Engineering Manual of Design and Construction of Levees (USACE, 2000), the first step in the levee design process is to "conduct geological studies based on a thorough review of available data including analysis of aerial photographs". However, this step is usually neglected especially in the non-federal and private sectors.

A levee breach can occur as a result of one, or a combination of triggering events such as overtopping, severe surface erosion and internal erosion within the levee body or foundation soils (Bogardi & Mathe, 1968). Moreover, less severe events such as slump slides can also threaten the integrity of levees. Slump slides are relatively shallow surficial instabilities on the river-side of levees which usually occur after a heavy rainfall with a long period of drying (Sills, 1983). This cycle of wetting and drying reduces the soil strength, and the excess water triggers the slump slide (Hossain et al., 2006). Such slump slides occur frequently along the Mississippi River levees. Many attempts have been made in recent years to employ remotely-sensed data to detect slump slides in early stages. Using multispectral and hyperspectral remotely sensed data and image classification (Hossain et al., 2006), developing slide prediction models by utilizing airborne hyperspectral imagery (Hossain and Easson, 2012), using PolSAR image with supervised and unsupervised algorithms (Aanstoos et al., 2012) and using in situ soil measurements for analysis of a PolSAR based classification of slump slides (Sehat et al., 2014a and 2014b) are examples of these attempts.

Many numerical and analytical investigations have been carried out to identify parameters that have more influence on levees instability. However, there are still several questions that remain unanswered regarding factors affecting the health of levees. A limited number of attempts have been made in the past years for the use of logistic regression in reliability analysis of levees. For example, Uno et al. (1987) investigated the application of a binary logit model for stability analysis of middle/small and large-scale levees. Without considering geological and geomorphological variables in the occurrence of a failure mechanism referred to as "outside slope failure", they took into account the effects of geometry, soil strength parameters and ratio of flow capacity to flood discharge. Using historical maps of the previous levee breach locations and historical datasets for site characteristics, Flor et al. (2010) utilized a regression model with a database of 76 levee breaches occurred along the Middle and Lower Mississippi River in the past 120 years to test the relative significance of geological, geomorphological, and other physical parameters on the vulnerability of the levee system. Heyer and Stamm (2013) discussed potential applications, advantages and limitations of regression models for reliability analysis of levees. Furthermore, while it is common to use for studying landslides, limited data exists in literature regarding the use of temporal analysis of precipitation data to demonstrate the relationship between rainfall and slump slides in levees. For example, Paudel et al. (2007) studied the amount and intensity of rainfall in several historical shallow landslides and showed that the occurrence of major landslide events coincided with rainfall peaks of heavy storms.

This study investigates the relevance and importance of rainfall and various geometrical and geomorphological factors to the vulnerability of earthen levees to slump

slides. The study is performed using data from 34 slump slides that occurred in the lower Mississippi River levee system over a time period of two years. In the first step, the precipitation data six months prior to the slump slides are collected and qualitatively evaluated to find its importance on the occurrence of the event. The study then takes a statistical analysis approach, logistic regression, to test the vulnerability of levees to slump slides due to various temporal and spatial parameters. This approach considers both quantitative and qualitative parameters. The binary logistic regression approach is utilized to investigate the correlation of some geological, geomorphological, physical and environmental factors on the occurrence of slump slides. The spatial factors considered in the model include the channel width, sinuosity index, location with respect to the channel shape, bank erosion, and distance to river. The spatial data used in the analyses was collected from airborne and satellite imageries along with field inspections. Identifying more influential factors on the occurrence of slump slides can help to locate high risk areas on levees for protective actions, closer monitoring and early response under emergency conditions.

Study area

The Mississippi River flows more than 3,700 km from its origin at Lake Itasca through the Gulf of Mexico. Its basin covers more than 3,224,000 km^2 that includes all or some parts of 31 states in the U.S. and two Canadian provinces. The lower Mississippi River refers to the part of the river starting from its confluence with the Ohio River down to the Gulf of Mexico. This study focuses on approximately 174 km of the main line levee system of the lower Mississippi River from near Clarksdale to Vicksburg in the

state of Mississippi (Figure 14). This area is under the jurisdiction of the Board of Mississippi Levee Commissioners.

An extensive set of in-situ and remotely-sensed data was collected for the study area through a research project which was recently completed at Mississippi State University (Aanstoos et al., 2012). The collected data includes in-situ soil properties, field observation reports, information about slump slides, aerial imagery from the Uninhabited Aerial Vehicle Synthetic Aperture Radar (UAVSAR), radar images from the TerraSAR-X satellite (Aanstoos et al., 2012, Sehat et al. 2014a).

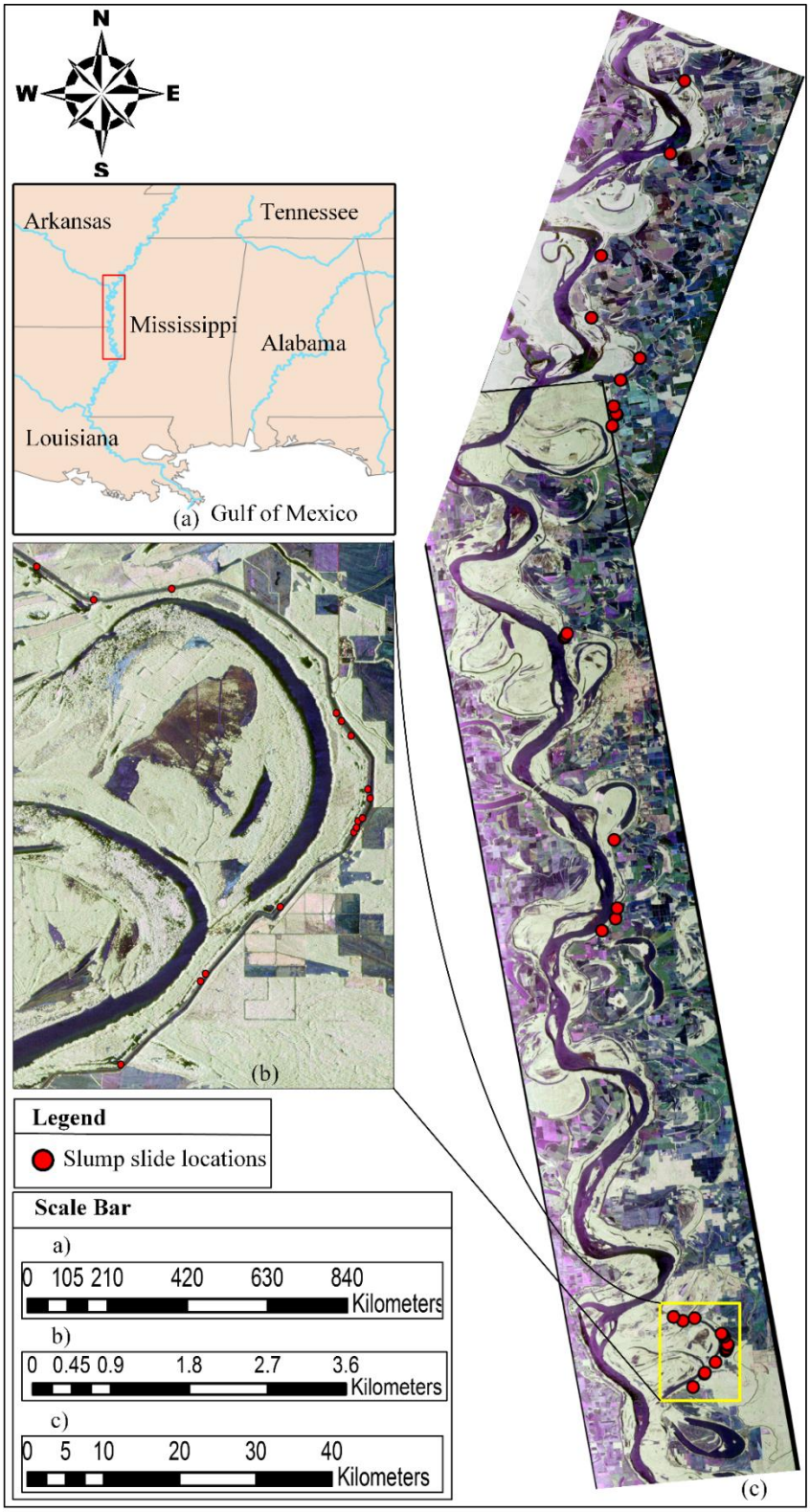

Figure 14 Study area (red rectangle) and slump slide locations (red dots)

Levee database

This study relies on a comprehensive dataset of 34 documented levee slump slides through the 174 km of the main line levee system of the Mississippi River collected by the U.S. Army Corps of Engineers (USACE), Mississippi Levee Board (2009) and our team during a time period of two years, 2008-9009. Table 2 presents the dataset for the current study and includes the information regarding the location, geometry, and approximate time of appearance and repair for most of the slides. The slides are shown by red circles in Figure 14. The length of the slides ranges between approximately 15 m and 76 m. The distance of the slide from the levee crown is between 0 to approximately 41 m and their vertical faces range between 0.3 and 4.57 m deep. Figure 15 displays a schematic view of a slump slide on levee, as well as a real slump slide. More than 80% of the slump slides occurred between April and October of each year. Specifically, more than half of the slump slides that occurred in 2008 and 75% of the slump slides that occurred in 2009 appeared between June and October of that year.

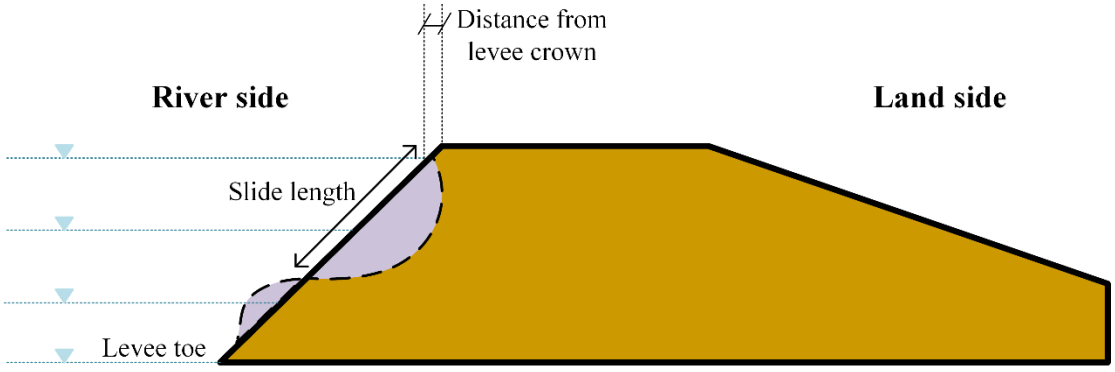

Figure 15 Schematic view of levee section with slump slide (modified after Hossain et al. 2006)

As can be seen in Table 2, the dates of appearance for some of the slump slides are not available, while at some points the slump slide appearance day and at other points the possible month of occurrence is available. The missing information is due to the relatively low frequency of levee inspections. Given the temporal accuracy of the available dataset, the precipitation analysis in this work and the developed regression model are based on monthly time steps. The same scenario applies to the slump slides repair date in the last column of Table 2.

Table 2 Levee slump slide dataset over the study area

Slide #	Length (m)	Vertical Face (m)	Distance from crown (m)	Position		Date Slide Appeared	Date Slide Repaired
				Latitude (North)	Longitude (West)		
1	42.67	0.61	12.19	N34-05'-59.4"	W90-52'-52.5"	-	-
2	21.34	0.91	4.57	N34-01'-03"	W90-54'-41.4"	-	-
3	18.29	0.61	19.81	N33-54'-39.1"	W91-00'-39.9"	June, 2009	-
4	27.43	1.22	3.05	N33-50'-24.5"	W91-02'-02.2"	Feb., 2009	April, 2009
5	21.34	0.91	1.52	N33-47'-02.3"	W90-59'-05.4"	May, 2008	April, 2009
6	76.2	1.83	7.01	N33-45'-42.7"	W91-00'-41.0"	June, 2008	April, 2009
7	32	0.91	12.8	N33-43'-57.4"	W91-01'-27.9"	12 Feb, 2009	Oct., 2009
8	64.01	1.52	7.32	N33-43'-24.1"	W91-01'-21.9"	7 Apr, 2008	Oct., 2009
9	45.72	0.61	0.3	N33-43'-19.0"	W91-01'-20.4"	21 Oct, 2008	Oct., 2009
10	18.29	2.44	0.3	N33-42'-36.7"	W91-01'-46.2"	Sept, 2008	Oct., 2009
11	18.29	0.61	14.32	N33-42'-33.5"	W91-01'-46.6"	-	Mar., 2010
12	33.53	0.91	0	N33-28'-13"	W91-06'-19.8"	Nov, 2009	Aug., 2010
13	45.72	0.91	7.62	N33-28'-03.2"	W91-06'-26.1"	-	Aug., 2010
14	53.34	0.91	0	N33-27'-56.9"	W91-06'-32.5"	-	Aug., 2010
15	22.86	0.3	3.66	N33-13'-19.4"	W91-04'-21.3"	-	-
16	22.86	0.3	19.81	N33-08'-28.6"	W91-04'-34.5"	13 Oct, 2008	-
17	41.15	4.57	3.66	N33-07'-44.4"	W91-04'-46.1"	Oct, 2009	Mar., 2010
18	27.43	0.91	21.34	N33-06'-58.5"	W91-05'-48.9"	12 Apr, 2008	-
19	33.53	0.61	9.14	N32-39'-11.7"	W91-03'-17"	-	Nov., 2009
20	36.58	2.13	0.61	N32-38'-51.4"	W91-02'-39.4"	20 Oct, 2009	Nov., 2009
21	-	-	15.24	N32-38'-58.2"	W91-01'-48"	26 Oct, 2009	Nov., 2009
22	30.48	3.05	0.91	N32-37'-42.1"	W90-59'-59.5"	Oct, 2009	Nov., 2009
23	70.1	2.13	2.74	N32-37'-37.2"	W90-59'-56.2"	21 Oct, 2009	April, 2010
24	57.91	0.45	36.57	N32-37'-28.2"	W90-59'-49.8"	-	-
25	33.53	0.61	41.15	N32-36'-55.4"	W90-59'-38.8"	-	-
26	50.29	0.61	4.57	N32-36'-49.9"	W90-59'-37.3"	21 Oct, 2009	Nov., 2009
27	24.38	0.61	9.14	N32-36'-37.7"	W90-59'-42.3"	21 Oct, 2009	Nov., 2009
28	27.43	0.61	42.67	N32-36'-36.0"	W90-59'-45.2"	-	-
29	36.58	0.91	4.57	N32-36'-32.0"	W90-59'-46.3"	Aug, 2008	Nov., 2009
30	60.96	2.44	2.44	N32-36'-29.1"	W90-59'-48.0"	-	Sept., 2010
31	15.24	0.3	28.65	N32-35'-43.4"	W91-00'-36.5"	Sept, 2009	April, 2010
32	21.34	0.3	30.48	N32-35'-02.4"	W91-01'-25.7"	-	Sept., 2010
33	24.38	0.61	30.48	N32-34'-57.9"	W91-01'-29.0"	-	Sept., 2010
34	38.1	0.91	6.09	N32-34'-06.9"	W91-02'-21.6"	Feb, 2009	Sept., 2010

Precipitation data

Precipitation plays a critical role in triggering slump slides in earthen levees. Higher rain intensity and/or longer rain duration can increase the degree of saturation within the body of the levee in a short time period. This results in a significant decrease in shear strength of the soil due to an increase of pore water pressure and loss of matric suction. In this section, the impact of rainfall within the six months of the slide was studied.

Data acquisition

The precipitation data studied in this work is collected from the "Observed Precipitation Data" from the National Weather Service (NWS) website. This data is a byproduct of NWS operations at the 12 CONUS River Forecast Centers (RFCs), and is displayed as a gridded field with a spatial resolution of about 4x4 km. This dataset is the output of algorithms that combine radar, gauge and satellite inputs which results in higher accuracy precipitation estimates than those which rely only on single sensors. According to the NWS, this dataset is one of the best available sources of timely, high resolution precipitation information. For the current study, monthly rainfall data from four neighboring points of each slide location was collected. The precipitation at the slide location was interpolated from those four points using the Kriging function of ArcMAP 10.1. This function measures the distances and directions between all possible pairs of sample points and creates the best fit surface.

Analysis of precipitation data

In order to investigate the impact of precipitation, monthly and cumulative monthly precipitation were plotted for each slump slide. As mentioned earlier, the amount of rainfall is an important factor triggering slump sliding in levees. For the 23 slump slides for which the precipitation data was examined, Table 3 summarizes the information pertaining the rainfall data in the month of slide as well as cumulative rainfall six months prior to the event. Figure 16 shows monthly and cumulative rainfall for each slide. From these it can be seen that the timing of 10 slump slides coincides with the month of peak rainfall in the past 6 months. Excluding Slide 8, nine of these (slides 5, 17, 20, 21, 22, 23, 26, 27 and 29) occurred in the month of maximum rainfall. Seven slides occurred one month after the peak rainfall month and the other six slides occurred two months after the peak rainfall month and in a drier month. Among these events, slide 17 which occurred in October 2009 had the maximum cumulative rainfall of 1254 mm, and slide number 8 which occurred in April 2008 had the minimum cumulative rainfall of 679.5mm.

Table 3 Summary of cumulative rainfall within the past six months of event occurrence and in the month of slump slide

Slide #	3	4	5	6	7	8	9	10
Cumulative rainfall (mm)	928.1	869.7	819.4	802.9	819.2	679.5	956.1	1007.4
Event month rainfall (mm)	29.2	83.3	209.3	37.6	60.2	135.9	51.8	169.4
Slide #	12	13	14	16	17	18	20	21
Cumulative rainfall (mm)	1183.4	1183.4	1183.4	1062.0	1254.0	708.9	1045.7	1069.8
Event month rainfall (mm)	58.9	58.9	58.9	33.3	355.3	100.3	293.3	293.1
Slide #	22	23	26	27	29	31	34	
Cumulative rainfall (mm)	1069.8	1069.8	1074.2	1069.6	856.5	971.3	963.7	
Event month rainfall (mm)	293.1	293.1	285.2	285.2	250.4	100.0	20.8	

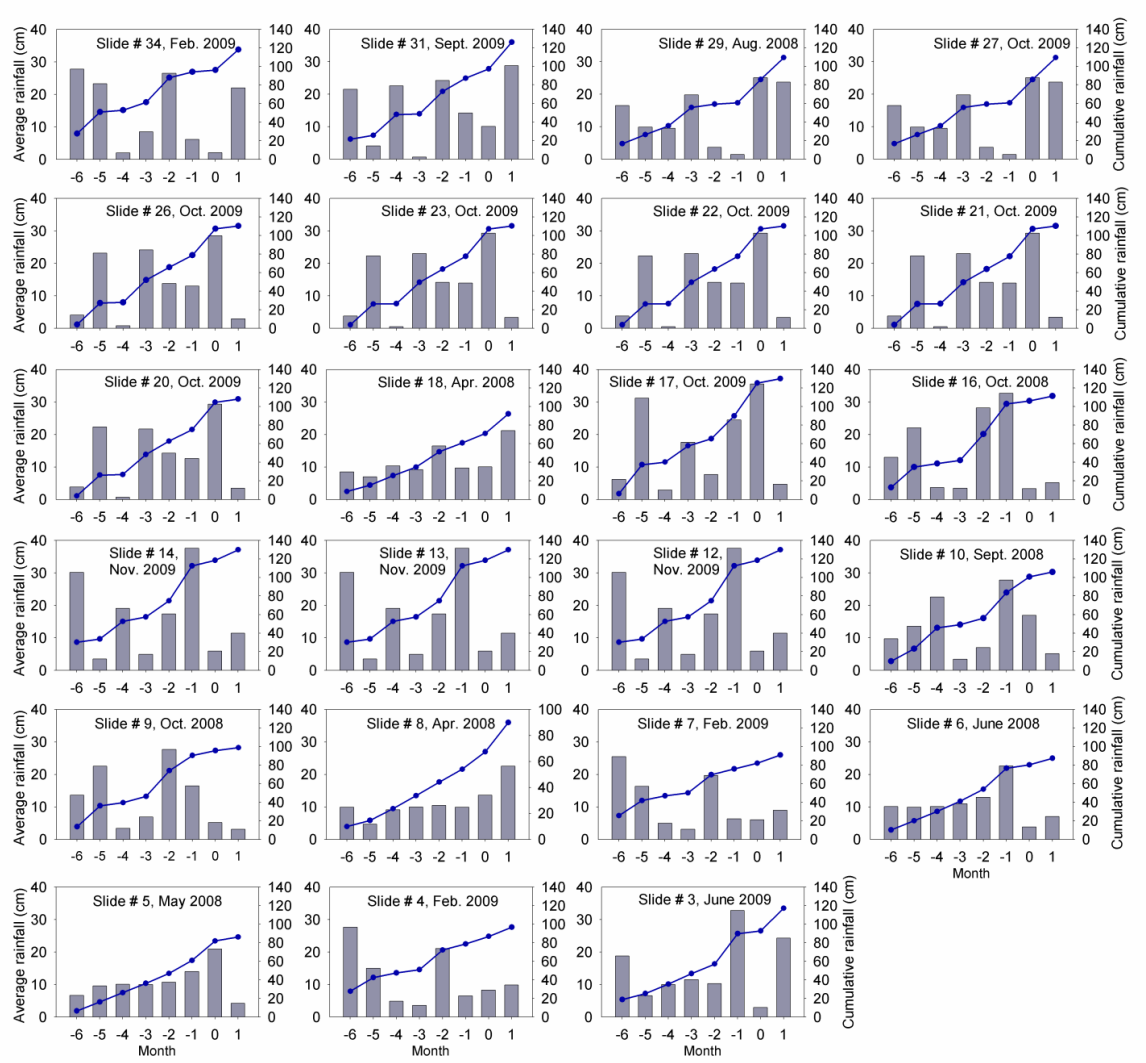

Figure 16 Monthly and cumulative rainfall for all slump slides (the x-axis shows the time from the month of slide)

The cumulative monthly rainfall curves are qualitatively tested for the 23 slump slides (Figure 17). These curves indicate the importance of rainfall gradient in the ultimate slump slide failure. The curves show an average gradient of 10 cm/month for the first 3-month time step, and a much steeper mean gradient of approximately 16 cm/month in the second 3-month time step before the slump slide event. Overall, it indicates an

intense rainfall in the 3 months prior to the slump slide event. Similar investigation has been implemented by Ibsen and Brunsden (2004) to study the relations between rainfall and landslides, and found that an approximate six month rainfall period is enough for landslide analysis in a homogeneous clay shales.

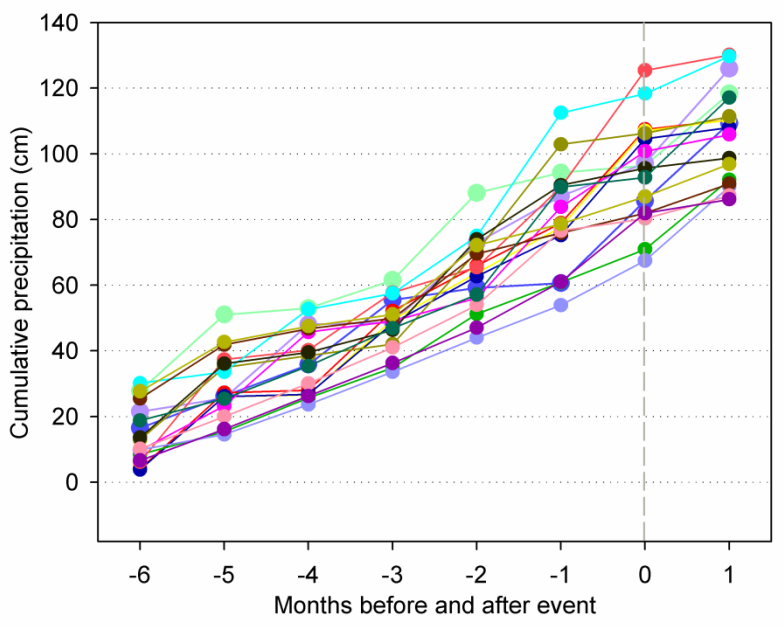

Figure 17 Six month cumulative rainfall for 23 slump slides in the study area

The results presented here are a qualitative assessment of the precipitation data and their potential impact in triggering slump slides in levees. Upon availability of additional data, further studies would be possible to quantitatively analyze rainfall time-series effects on slump slide failures at finer time scales. For example, for those slides for which exact appearance date is available (7, 8, 9, 16, 18, 20, 21, 23, 26 and 27), such analysis could be performed on a daily time scale within the past week of the event rather than merely within the past 6 months. Such higher resolution precipitation data could

reveal relationships between peak rainfall days and slump slide occurrence. Moreover, a rainfall threshold could be determined for the slump slide occurrence. However, such 24-hr precipitation data was not available through the NWS Precipitation Dataset for the study area.

Geometrical and geomorphological variables

In addition to the precipitation data, this work investigates the impact of various geometrical and geomorphological variables through a series of regression analyses. Selecting appropriate independent variables is a critical step in the regression analysis. The variables should be selected in such a way that they capture the most influencing factors on slump slides to obtain the best model fit (Heyer & Stamm, 2013). In the following sections, each independent variable used in the model is discussed in detail. Most of the site characteristics are derived from investigating the NASA UAVSAR imagery acquired on January 25, 2010 as well as the National Agriculture Imagery Program (NAIP) aerial imagery of 2012 over the study area.

It is worth noting that many other parameters besides the ones used in this study can possibly stimulate slump slides in levees. Such parameters include human activities, earthquakes, engineering characteristics and behavior of the levee soil, vegetation type, etc. However, such data did not exist for the levees in the study area which are mostly built by piling soil, clay, sand, or rocks borrow pits.

Channel width

Channel characteristics such as the channel width, channel depth and meander bends are important factors that influence channel capacity and stability as well as flow

velocity. Channel modification operations such as deepening and widening the channel, and cutting off meanders are commonly conducted along the Mississippi River for flood control purposes (Shankman and Smith, 2004). The Mississippi River significantly varies in width and historical flood data shows that water surface velocity and divergence magnitude is larger in narrower banks and apexes (Hattori et al. 2009). In other words, because of their smaller cross sectional areas, they are more prone to flood due to the hydrodynamic regime coming from a period of heavy or long-lasting rainfall. A higher chance of flooding translates to a higher chance of levee failures and instabilities.

In the current study, the channel width is selected as a binary independent variable. It is investigated whether or not the slump slides have occurred more in the locations where the channel width is larger than 1,000 m. This threshold value is selected according to a study conducted for assessing unfavorable parameters to identify vulnerable areas on the same study area (Hassan, 2011).

Channel sinuosity index

The sinuosity index between two points of a river is the ratio of the length of the river curve and the straight distance between the two points. This parameter is a strong indicator of channel dynamics, which controls channel stability (Lane, 1995). Flor et al. (2010) found that levee breaches that occurred along the Lower Mississippi River had a noticeable correlation with the river sinuosity index. Fisk's (1944) and Saucier's (1994) efforts on a broad wealth of materials about the Mississippi River imply that the river has significantly changed its path over long periods of time. Meander bends within the sinuous channel have been changed into oxbow lakes mostly by neck cut-offs. In this study, the sinuosity index is measured according to the current condition of the river after

transformations from meander bends to oxbows. In most cases, aerial imagery is used to calculate the sinuosity index (e.g., Rosgen, 1994, Flor et al., 2010). There are different river classifications available based on the sinuosity, width/depth ratio, etc. Natural rivers classification based on sinuosity are usually in the form of low, moderate, high and very high sinuous rivers (Rosgen, 1994). Considering the morphology of the study area, the sinuosity index is classified into winding (<1.25), twisty (1.25 ~ 1.50) and meandering (>1.50) in the current study.

Location with respect to channel shape

Meander bends are historically considered as one of the undesirable factors triggering levee instabilities. Cutting off meander bends is one of the primary actions that has taken place since the 1927 flood over the Lower Mississippi River (USACE, 2014). More than 250 km of the channel has been straightened under this action (Shankman and Smith, 2004, Hudson et al., 2008). About 76% of the levee scours that happened in the Missouri River levee system during the 1993 flood occurred along meander cut banks (Galat et al., 1997). Also, the levees of Lower Mississippi River located on meander cut banks are found to be 2.3 times more likely to fail than those located along the straight portion of the river (Flor et al. 2010).

The Lower Mississippi River, from Cairo, IL to Red River Landing, is a laterally migrating meandering channel within the alluvial valley (Fisk, 1944; Schumm et al., 1994; Wasklewicz et al., 2004). According to the morphology of the study area, the channel shape is categorized into three possible groups in the sites: meander bends, oxbow lakes and straight channel.

Riverbank erosion

Riverbank erosion is primarily controlled by antecedent moisture, texture and vegetation cover (Simon et al., 1999, Henshaw, et al., 2013). According to Nagata et al. (2000), riverbank erosion usually involves four steps: bed scouring at the side bank, collapse due to instability of the scoured bank, deposition of the collapsed bank materials, and the movement of the deposited materials. Rate of riverbank erosion increases during flooding times (Knighton, 1973). Therefore, studying riverbank erosion around the slump slide locations may help identifying vulnerable areas. In this study, riverbank erosions are modeled and drawn by visual interpretation, comparing Landsat and TerraSAR imagery acquired in September 2010 over the study area. This variable represents a qualitative identification of the areas where erosion has taken place.

Distance to water

Hasan et al. (2011) showed that most of the slump slides occurred in this study area have been in close proximity to the river or water. This variable is selected to be examined in the regression model because areas closer to the water are more susceptible to be exposed by floodplain areas and are more prone to experience flooding at the time of high water levels. This parameter is defined as the shortest distance from the toe of the levee to the river. It was measured using the UAVSAR imagery of the study area.

Logistic regression model

The main goal of regression analysis is to look for the relation between a dependent variable and a number of independent variables. The current study employs multiple spatial variables, including both categorical and numerical predictors, in a

logistic regression model to investigate the relevance and importance of the parameters to slump slide occurrence on levees (i.e., dependent variable). The main advantage of logistic regression analysis is the capability of using both qualitative and quantitative variables. As the vulnerability of the levee system to slump slide can only have two possible outcomes (i.e., slide or non-slide occurrence in levee), it is defined as a binary dependent variable in the regression analysis. For example, for assessing whether or not the channel width or sinuosity index ratio has affected the health of levee, the dependent variable is coded 1 at the locations where a slump slide has occurred and 0 when it has not occurred.

For the dependent variable of the regression model, this study uses the record of 34 slump slides (reported in Table 2) that occurred in a time period of two years from the beginning of 2008 until the end of 2009. Since the 34 slump slides have occurred through a long length of the river (174 km), the number of points with a dependent variable of "1" (i.e., occurrence of side) is much lower than the points with the dependent variable of "0" (i.e., non-occurrence). Such condition in regression analysis is referred to as rare events data (King and Zeng, 2001). Since the contribution to the independent variables' information content for each additional zero drops as the number of zeroes exceeds the number of ones, it is recommended to use "0" dependent variables no more than two to five times more than "1" dependent variables (King and Zeng, 2001). Therefore we randomly collected a total number of 68 (34×2) healthy sites (i.e., sites with no record of slump slide). The healthy sites were collected using a random generation of mileage from the length of the levee. In general, logistic regression analysis works better with large data sets. With this in mind, we selected the number of non-slump slide sites to

be two times the number of slump slide sites in order to create a larger dataset and to improve the performance of the regression analysis.

We then employed the five variables discussed in the previous section to characterize all of the 102 healthy and slump slide sites. The spatial variables which were used in the logistic regression model include the channel width, channel sinuosity index, location with respect to channel shape, riverbank erosion, and distance to water. Table 4 shows the list of variables, type of each, and their most appropriate classification for the model. Independent variables such as riverbank erosion or sinuosity index are classified into categorical variables, meaning that they can be assigned a fixed level from a number of feasible values. Levels assigned to each variable are shown using two-letter codes. Classification of levels for the variables are described in details in the previous section. The only numerical variable, distance to river, can take different values and numbers.

Table 4 Variables used in the logistic regression model

Code	Variable	Type	Level Code	Level
W	Channel width	Categorical	WL	< 1000 m
			WM	> 1000 m
S	River sinuosity index	Categorical	SW	1.05 ~ 1.25
			ST	1.25 ~ 1.50
			SM	> 1.50
L	Location with respect to channel shape	Categorical	LM	Meander bend
			LO	Oxbow lake
			LS	Straight
E	Riverbank erosion	Categorical	EY	Yes
			EN	No
D	Distance to water	Numerical	-	-

The weighted average distribution for each independent variable can be seen in Figures 18 and 19. Chart "a" in figure 5 shows almost a uniform distribution in channel sinuosity index between all possible outcomes. 22% of all cases (slides and non-slides) are slides with twisting sinuosity index, and the rest of cases with slides that are approximately equally distributed between winding and meandering sinuosity index. Chart "b" shows that 23.6% of all cases are slides that have riverbank erosion, while 38.9% of all cases are non-slide areas with no riverbank erosion. According to chart "c", 41.2% of all the cases are slides with a corresponding channel width of less than 1000 m. Chart "d" shows that 32.3% of all cases are slump slides which are located on ox bow

lakes, while only 1.5% of them locate on straight portions of river. On the other hand, 29.5% of all cases are non-slide areas that locate on straight portions of river, and the rest of non-slides are almost equally divided between meandering portions of river and ox bow lakes.

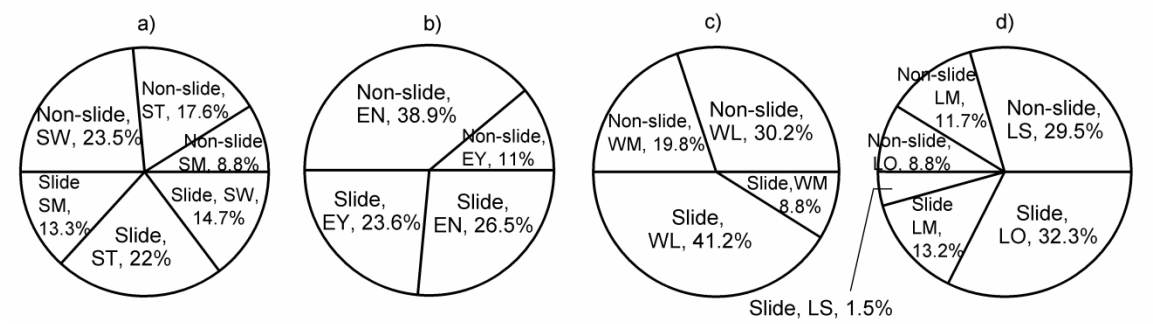

Figure 18 Pie chart distribution for qualitative variables: a) Channel sinuosity index, b) Riverbank erosion, c) Channel width, d) Location with respect to channel shape

Figure 19 shows the data distribution for the numerical variable distance to water. More than 70% of non-slide locations are located more than 1000 m away from the water, while approximately 80% of slide areas are located in less than 1000 m from the water.

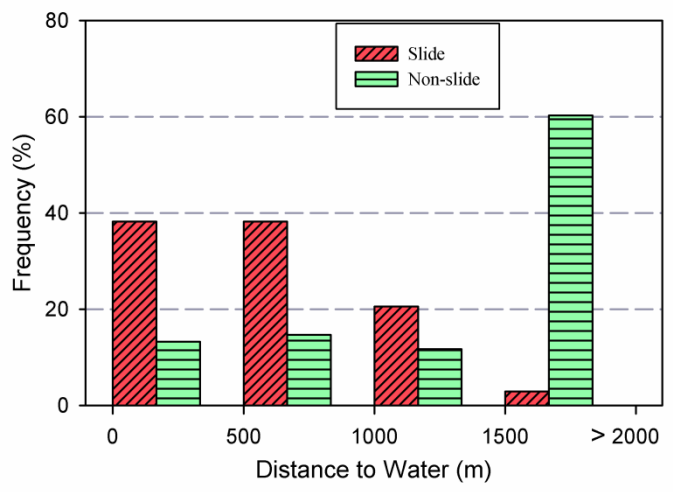

Figure 19 Data distribution for the numerical variable "Distance to water"

The model is implemented using the binary logistic regression function of Minitab 17. The first model includes all the variables while the second model, which is developed based on the findings from the first model, includes four variables. The Pearson and Deviance tests are used to assure the goodness-of-fit of the logit model.

Results and discussion

Regression model with all variables

After running the model, the first step is to compare the obtained P-values to the α level. Fisher (1925) suggested a probability of one in twenty (α level of 0.05, or significance level of 95%) as a conservative cutoff level to reject the null hypothesis. However, he recommended later to set the significance level according to circumstances of the project (Quinn and Keough, 2002). In this section, the significance of each variable was tested using an α level of 0.05 in order not to take high risks of making a wrong decision. The p-value specifies whether there is a statistically significant association

between each predictor variable and the response variable. P-values for each predictor is shown in Table 5. The model has an R2 value of 39.02%, and the predictor channel sinuosity index is the variable that does not meet the significance threshold of P-value = 0.05.

Table 5 Results of the regression model

Variable	P-Value
Channel width	0.044
Riverbank erosion	0.001
Channel sinuosity index	0.285
Location with respect to channel shape	0.013
Distance to water	0.029

The odds of an event equal the probability that the event occurs divided by the probability that it does not occur. Therefore the odds ratio compares the odds of each two levels (here Levels A and B) of a predictor (Table 6). Based on this definition, Levels A and B are set for each independent variable to show odds ratio. For example, the odds ratio for a location on a levee whose channel width is more than 1,000 meters is 0.237, meaning that the slump slides happen 4.219 times more in the areas with a channel width less than 1,000 m. The odds ratio of the riverbank erosion variable suggests that the slump slide failure is 9.75 times more likely to occur if riverbank erosion is detected there compared to the sites without riverbank erosion. As for sinuosity level, the results suggest that a slump slide is 0.487 times more likely to appear on parts of the levee with a corresponding river sinuosity level of twisty compared to sinuosity level of meandering.

In other words, the areas with a meandering level are 2.053 times more likely to be prone to slump slides in comparison to the twisty level. A slump slide is 0.269 times more likely (3.717 times less likely) to appear on parts of the levee where the corresponding river sinuosity level is winding in comparison to meandering. Finally, a slump slide is 0.552 times more likely (1.811 times less likely) to appear on parts of the levee with a corresponding river sinuosity level of winding than with a level of twisty, which means that a slump slide is 1.811 times more likely to occur on twisty parts of the levee system than winding ones.

The odds ratio of the location with respect to the channel shape variable suggests that a slump slide on levee is 6.707 times more likely to occur on oxbow lakes compared to meander bends. It also shows that a levee slump slide is 0.642 times more likely to happen on straight portions of river rather than meander bends, which means that meander bends are 1.557 times more prone to slump slides than straight portions. The results show that oxbow lakes are 10.438 times more prone to slump slide failure than straight portions of river. As for the distance to water variable, for each additional 100 m distance from the levee toe to the water, the odds that a slump slide occurs decrease by 6%. In other words, for each 100 m units of becoming closer to the water, the odds of slump slide failure increase by 6% (Table 6).

Table 6 Summary of odds ratio for level A relative to level B for categorical predictors, and odds ratio for continuous predictor

Categorical Predictors		
Level A	Level B	Odds Ratio
Channel width (More)	Channel width (Less)	0.237
River sinuosity index (Twisty)	River sinuosity index (Meandering)	0.487
River sinuosity index (Winding)	River sinuosity index (Meandering)	0.269
River sinuosity index (Winding)	River sinuosity index (Twisty)	0.552
Riverbank erosion (Yes)	Riverbank erosion (No)	9.750
Location with respect to channel shape (Oxbow)	Location with respect to channel shape (Meander bend)	6.707
Location with respect to channel shape (Straight)	Location with respect to channel shape (Meander)	0.642
Location with respect to channel shape (Straight)	Location with respect to channel shape (Oxbow)	0.096
Continuous Predictor		
Distance to water	Unit of change: 100 m	0.941

In binary logistic regression, the probability of slump slide occurrence (= 1) at a specific location is derived based on:

$$\mathrm{P}\,(1) = \frac{\exp(y\prime)}{1+\exp(y\prime)} \tag{2}$$

where

$$y' = \beta_0 + \sum \beta_i x_i \tag{3}$$

where x_i observations are the known predictors, and β_i is the estimated regression coefficient. The regression equation which is used to describe the relationship between the response and predictor variables is derived as:

$$Y' = 0.074 - 0.000605D + 1.439WL - 2.277EN + 0.718SM - 0.593SW + 1.903LO – 0.442LS \quad (4)$$

Regression model without river sinuosity index

The regression analyses was performed again after excluding the river sinuosity index variable as its corresponding P-Value was more than the α level. The new model has an R2 value of 37.08%. The Pearson and deviance test was used to assure the goodness-of-fit of the logit model. The P-Values for predictors are shown in Table 7.

Table 7 Results of the new regression model

Variable	P-Value
Channel width	0.014
Riverbank erosion	0.002
Location with respect to channel shape	0.015
Distance to water	0.079

The odds ratio for a location on levee whose channel width is more than 1,000 meters is 0.195, meaning that slump slides happen 5.128 times more in areas with channel width less than 1,000 m. The odds ratio of the riverbank erosion variable suggests that levee slump slide failure is 8.768 times more likely to occur if riverbank erosion is detected there compared to sites without riverbank erosion. The odds ratio of the location with respect to channel shape variable suggests that slump slide failure on levee is 3.817 times more likely to occur on oxbow lakes compared to meander bends. Levee slump slide failure is 0.347 times more likely to occur on straight portions of the river rather than meander bends, which means that meander bends are 2.881 times more likely to experience slump slide failure than straight portions. It then suggests that oxbow

lakes are 10.976 times more prone to slump slide failure than straight portions of river. As for the numerical variable distance to water, for each additional 100 m distance from the levee toe to the water, the odds that a slump slide occurs decrease by about 4%. In other words, for each 100 m becoming closer to the water, the odds of slump slide failure increase by about 4% (Table 8).

Table 8 Summary of odds ratio for level A relative to level B for categorical predictors, and odds ratio for continuous predictor in the new model

Categorical Predictors		
Level A	Level B	Odds Ratio
Channel width (More)	Channel width (Less)	0.195
Riverbank erosion (Yes)	Riverbank erosion (No)	8.768
Location with respect to channel shape (Oxbow)	Location with respect to channel shape (Meander bend)	3.817
Location with respect to channel shape (Straight)	Location with respect to channel shape (Meander)	0.347
Location with respect to channel shape (Straight)	Location with respect to channel shape (Oxbow)	0.091
Continuous Predictor		
Distance to water	Unit of change: 100 m	0.960

Regression equation according to the new set of predictors:

$$Y' = -0.030 - 0.000419D + 1.634WL - 2.171EN + 1.340LO - 1.056LS \quad (5)$$

Single variable regression equations

Using the regression analyses which were discussed in the previous section (i.e., after excluding river sinuosity), a separate regression equation is provided for each level

of each categorical predictor of the regression model to find the most and the least vulnerable locations in the study area. The relative probabilities of the groups can be evaluated with a comparison of the constant values in the equation. Table 9 shows the individual equations for different qualitative variables. There we have 12 equations as there are two predictors with 3 levels, and one predictor with two levels. Since the distance to the river predictor is numerical, the coefficient corresponding to this predictor is the same in all the equations. According to Table 9, the levee sections with a corresponding width of river less than 1,000 m, riverbank erosion detected channel bed, and located on oxbow lakes are the most vulnerable areas for failure with the highest positive constant value of 2.944. The least vulnerable area for slump slide occurrence are areas located more than 1,000 m away from the water, with no riverbank erosion at the channel bed and on straight portions of the river. Such a model resulted in an intercept of -3.258.

Table 9 Separate equations for variables

W	E	L	Regression Equation
Less	Yes	Oxbow	Y' = 2.944 – 0.000419 D (6)
		Meander	Y' = 1.604 – 0.000419 D (7)
More		Oxbow	Y' = 1.309 – 0.000419 D (8)
Less	No		Y' = 0.7726 – 0.000419 D (9)
	Yes	Straight	Y' = 0.5481 – 0.000419 D (10)
More		Meander	Y' = –0.03020 – 0.000419D (11)
Less	No		Y' = –0.5670 – 0.000419D (12)
More		Oxbow	Y' = –0.8618 – 0.000419D (13)
	Yes	Straight	Y' = –1.086 – 0.000419D (14)
Less	No		Y' = –1.623 – 0.000419D (15)
More		Meander	Y' = –2.201 – 0.000419D (16)
		Straight	Y' = –3.258 – 0.000419D (17)

The model is then used to predict the probability of slump slide occurrence for the most and the least vulnerable areas according to Table 9. For example, the fitted probability that a slump slide occurs on a specific location of levee with the corresponding water width of less than 1,000 m, with detected riverbank erosion, located on an oxbow lakes, with a 900 m distance to water, is predicted to be 92.9% with a standard error of 0.054. It is estimated that with 95% confidence, the probability of slump slide occurrence in this location is between 72.13% and 98.45%. On the other hand, for the least vulnerable location where it is assumed to be 1,500 m away from the water, with

corresponding water width of more than 1,000 m, no riverbank erosion detected, and located on the straight portion of the river, the fitted probability is predicted to be 2.01% with a standard error of 0.018. It is estimated that with 95% confidence, the probability of slump slide occurrence in such location is between 0.33% and 11.08%.

Model verification

In order to verify the logistic regression model which was developed in this study, the model's performance was examined for two new data points which were not included in the regression analysis: one case of slump slide and one case of non-slide. The slump slide is reported that occurred in June, 2010 on the west side of the Lower Mississippi river levee system in the state of Louisiana, and the location of the non-slide point is randomly selected. The locations and predictive variables of the slump slide and non-slide points used for verification purposes are shown in Figure 20 and Table 10, respectively.

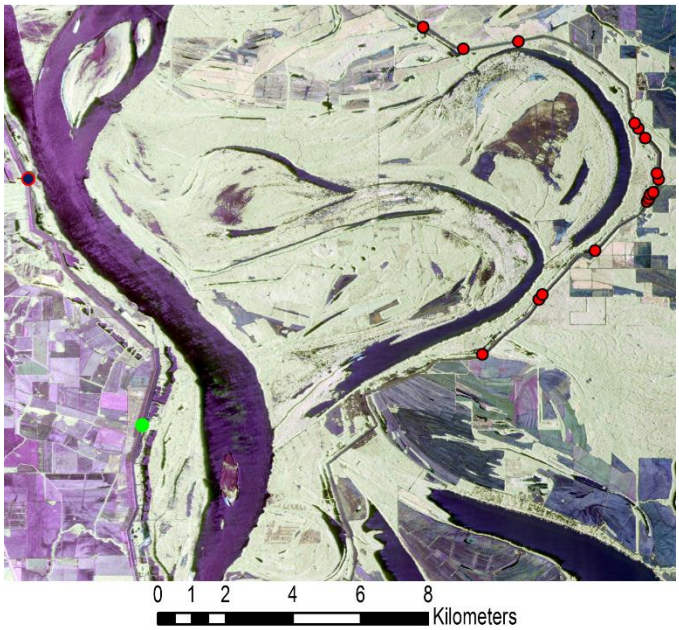

Figure 20 Locations of the slump slide (dark blue dot) and non-slide (green dot) cases used for verification. Red dots are the slump slides which were used in the regression analysis.

Table 10 Predicted variables for the slide and non-slide cases used for verification

Predictor variables	Case a: Slide (1)	Case b: Non-slide (0)
Riverbank erosion	EY	EN
Location with respect to channel shape	LO	LM
distance to water	1400 m	1400 m
water width	WM : 1170 m	WM : 1600 m
y'	0.7234	-2.7876
$e^{y'}$	2.0614	0.0615
P(1)	0.6733	0.0579

The results shown in Table 10 indicate that the model could reasonably predict the probability of slump slide occurrence for both cases which were tested. As shown, the developed regression model predicts probability of 67.3% and 5.8% of slide occurrence

for the slump slide and no-slide points, respectively. Since the model predicts a high probability of occurrence in the slide location, this area and other areas with such high probability need to be in the top priority for monitoring.

CHAPTER IV

CONCLUSION

Summary of work accomplished for using in situ soil measurements for analysis of classified UAVSAR imageries of levee slump slides

In this work statistical analyses were performed to compare soil properties of different classes from the output of an earthen levee slump slide classifier. Although "false positive" is defined as a commission error of a classifying system, this study investigated the vulnerability of false positives from an unsupervised levee slump slide classifier to future failures. This task was accomplished by comparing soil texture, moisture content, hydraulic conductivity and penetration resistance in different classes of the classifier output as contributing factors for slump slides in levees.

Two methods of analysis were used: pixel-based and object-based. For the first method, the soil property distribution of all pixels classified as false positive was compared with that of all the slide and healthy area pixels. The comparisons demonstrated that the false positives exhibited similar trends in soil properties to the slide area in the surface layer. In the second method, this comparison was made between the pixels of two dense false positive zones with that of the slide and healthy areas. These dense false positive zones were selected based on the fact that their geometries looked like the slide area, and also the classifier's output in these zones had similar values to those in the slide area. The results of analyses obtained from the object-based method,

and the later discovery of cracks and stressed vegetation in one of these dense false positive zones, indicate the importance of this study. The results presented here could potentially help engineers and levee managers to find high risk areas and repair the most needed ones in advance. However we believe that further investigation is needed to strengthen this conclusion.

Summary of work accomplished for effects of rainfall and other variables on vulnerability of levee system to slump slides

Levees systems provide flood protection in various regions in the U.S. and all around the world. Continuous assessment of the levee's integrity and monitoring their health under various normal and extreme loading conditions is a critical task which warrants further attention to improve currently available methods. The integrity of a levee can be fully or partially threatened by instabilities in the levee's body or foundation.

The current study focused on a shallow instability, referred to as slump slide, which commonly occurs on the river-side of earthen levees. Rainfall data and five other geometrical and geomorphological parameters for a database of 34 slump slides which occurred along the Lower Mississippi River levee system between 2008 and 2009 were investigated. The rainfall data was collected at the month of event as well as for the past six months before the slide event. The precipitation data was examined and the results showed that 9 out of 23 slump slide failures with clear observation dates happened in the peak rainfall month, 66% higher than average cumulative rainfall. Seven slides occurred one month after the peak rainfall month, with more than 70% higher than average cumulative rainfall, and the remaining six slides occurred two months after the peak rainfall month and in a drier month. A steep gradient in the cumulative rainfall was

observed for the three-month duration (0.62) before slump slide occurrence date in comparison to the previous three-month duration (0.40). The trend in the curves indicated that precipitation development is significant before slope instability occurrence.

Five geometrical and geomorphological parameters including the channel width, distance to water, channel sinuosity index, riverbank erosion detection, and the location with respect to channel shape were tested in a series of logistic regression analyses. Excluding sinuosity index in the first test, the α level of 0.05 and the P-Values less than α level in both tests reject the null hypothesis. With less than 95% significance level, sinuosity index was removed from the first model. This was rational according to the nature of the river in the study area; that it has high sinuosity in all parts of the study area and thus the variable is not an influencing factor in the model. The second model suggests that among the qualitative variables, the availability of riverbank erosion around the slides locations is the most significant predictor factor. Rate of riverbank erosion is directly related to the flood times and is a good indicator of vulnerable areas to flooding. Channel width less than 1,000 m wide, due to the lack of capacity to contain large volumes of water and thus an increase in the hydrodynamic regime in flood conditions is ranked the second most significant variable. Oxbow lakes were 10.976 and 3.817 times more prone to slump slide than straight portions of the river and meander bends, respectively. Meander bends were 2.881 times more prone to slump slide failure rather than straight portions of river. Finally, each additional 100 m distance from the levee toe to the water resulted in a 4% less probability of failure. The verification results showed that the model can reasonably predict the probability of slump slides for both slide and non-slide areas. It is anticipated that using a larger database of slump slide events and

considering more predictor variables can further improve the performance of the regression model. Overall, the results suggest that designers consider geological and environmental parameters in designing levees for future, and could assist decision-makers to identify the most vulnerable locations for slump slide failure on levees, in order to guide the allocation of monitoring or preventive activity.

Recommendations for future research

It is important to note the limitations involved in conducting this research. As for the first part of this work, larger studies to screen greater area with targeted intense inspections can be one of the best ways to expand the target classification to include non-visible areas of slope instability. Furthermore, other in situ measurements including more geotechnical parameters can be analyzed on the soil of the levee. Moreover, slope stability analysis for suspected areas can be conducted in structural scale using different methods like the Limit Equilibrium or Finite Element Method in order to find a factor of safety against slump slide instability. Also Discrete Element Method can be used to compute the motions and effects of each soil particle.

As for the second part of this work, it is worth noting that there are many other parameters besides the ones used in this study that can possibly stimulate slump slides in levees. Such parameters include human activities, earthquakes, engineering characteristics and behavior of the levee soil, vegetation type, etc. Considering these parameters in developing such regression analyses could result in a rich and more general regression model. Moreover, upon availability of additional data, further studies can be conducted for quantitative analyses of rainfall time-series effects on slump slide failures at finer time scales. For example, for those slides with available appearance date such

analysis can be performed on a daily time scale within the past week of the event rather than merely within the past 6 months. This higher resolution precipitation data can help to reveal relationships between peak rainfall days and slump slide occurrence

REFERENCES

Aanstoos, J.V., Dabbiru, L., Gokaraju, B., Hasan, K., Lee, M. A., Mahrooghy, M., Nobrega, R.A.A., O'Hara, C. G., Prasad, S., Shanker, A., 2012. Levee assessment via remote sensing SERRI Projects, SEERI Report 80023-02.

Abdoun, T., Bennett, V., Desrosiers, T., Simm, J., Barendse, M., 2013. Asset management and safety assessment of levees and earthen dams through comprehensive real-time field monitoring J. Geotech. Geol. Eng. 31, 833–843.

Ashton, E. A., Schaum, A., 1998. Algorithms for the detection of sub-pixel targets in multispectral imagery, Photogram. Eng. Remote Sens. 64, 723–731.

Bennett, V., Lv, X., Zeghal, M., A.M. ASCE, Abdoun, T., Yazici, B., Marr, A., 2014. Multi-scale Monitoring for Health Assessment of Levees in New Orleans, Geo-Congress, Atlanta, GA, Feb 23-26.

Bhowmik, N.G., et al., 1994. In: Buck, A.G., Changnon, S.A., Dalton, R.H., Durgunoglu, A., Semissie, M., Juhl, A.R., Knapp, H.V., Kunkel, K.E., McConkey, S.A., Scott, R.W., Singh, K.P., Soong, T.D., Sparks, R.E., Visocky, A.P., Vonnahme, D.R., Wendland, W.M. (Eds.), The 1993 Flood on the Mississippi River in Illinois: Illinois State Water Survey, Champaign, Miscellaneous Publication, 151.

Bogardi, I., Mathe, Z., 1968. Determination of the degree of protection offered by flood levees and the economic improvement thereof, National Water Authority, Department for Flood Control and River Training, Budapest, Hungary.

Campbell, J. B., 2007. Image classification, in: Introduction to remote sensing, fourth ed. A Division of Guilford Publications, Inc., New York, NY, pp. 324 – 366

Castillejo-González, I. L., López-Granados, F., García-Ferrer, A., Pe˜na-Barragán, J. M., Jurado-Expósito, M., Sánchez de la Orden, M., González-Audicana, M., 2009. Object- and pixel-based analysis for mapping crops and their agro-environmental associated measures using QuickBird imagery, Computers and Electronics in Agriculture. 68, 207–215.

Cedergren, H. R., 1989. Seepage, drainage, and flow nets, 3rd Ed. Wiley, New York.

Chang, C-I., Chiang, S-S., 2002. Anomaly detection and classification for hyperspectral imagery, IEEE Transactions on Geoscience and Remote Sensing. 40(6), 1314-1325.CRS, 2011. Locally operated levees: Issues and federal programs. Congressional Research Service, Available in: https://www.fas.org/sgp/crs/misc/R41752.pdf.

CRS, 2011. Locally operated levees: Issues and federal programs. Congressional Research Service, Available in: https://www.fas.org/sgp/crs/misc/R41752.pdf

Dabbiru, L., Aanstoos, J.V., Mahrooghy, M., Li, W., Shanker, A., Younan, N.H., 2012. Levee anomaly detection using polarimetric synthetic aperture radar data. IGARSS 2012, July 22–27, Munich, Germany.

Dupray, S., Tourment, R., Pohl, R., Schelfhout, H., Williamson, T., Gamst, K., Sharp, M., 2010. International Levee Handbook—Scoping Report, London, U.K.

Fell, R., Fry, J.J., 2013. An overview of the internal erosion process as it affects dams and levees, in: Bonelli, S. (Eds.), Erosion in Geomechanics Applied to Dams and Levees. John Wiley & Sons Inc., Hoboken, NJ, pp. 18-116.

Fisher, R. A., 1925. Statistical methods for research workers. Edinburgh, UK: Oliver and Boyd. ISBN 0-050-02170-2.

Fisk, H. N., 1944. Geological Investigation of the Alluvial Valley of the Lower Mississippi River, Vicksburg: Mississippi River Commission.

Fisk, H. N., 1944. Geological Investigation of the Alluvial Valley of the Lower Mississippi River, Vicksburg: Mississippi River Commission

Flor, A., Pinter, N., Remo, J.W.F., 2010. Evaluating levee failure susceptibility on the Mississippi River using logistic regression analysis, Eng. Geol. 116, 139–148

Galat, D. L., Kubisiak, J. F., Hooker, J. B., Sowa, L. M., 1997. Geomorphology, distribution and connectivity of lower Missouri River floodplain waterbodies scoured by the flood of 1993, Verh. Internat. Verein. Limnol. 26, 869-878

Grunwald, S., Lamsal, S., 2006. The impact of emerging geographic information technology on soil-landscape modeling, in: Grunwald, S. (Eds.), Environmental Soil-landscape: geographic information technologies and pedometrics. CRC Press 2006, Florida, 128–148.

Grunwald, S., Lowery, B., Rooney, D.J., McSweeney, K., 2001a. Profile cone penetrometer data used to distinguish between soil materials. Soil and Tillage Research. 62, 27–40.

Grunwald, S., McSweeney, K., Rooney, D.J., Lowery, B., 2001b. Soil layer models created with profile cone penetrometer data. Geoderma. 103, 181–201.

Hasan, K., Aanstoos, J. V., Mahrooghy, M., Dabbiru, L., Dunbar, J. B., 2011. Characterizing Mississippi River levee segments using soils and geologic data. Symposium on the Application of Geophysics to Engineering and Environmental Problems, April 2011. Available online at: http://www.hpc.msstate.edu/publications/docs/2011/01/8717SAGEEP_2011_KH.pdf

Hattori, K., Ishigaki, T., Ueno, T., 2009. Influence of Channel Width on the Flood Flows in a Stream Valley. Advances in Water Resources & Hydraulic Engineering. Proceedings of 16th IAHR-APD Congress and 3rd Symposium of IAHR-ISHS, 987–992.

Henshaw, A. J., Thorne, C. R., Clifford, N. J., 2013. Identifying causes and controls of river bank erosion in a British upland catchment. CATENA 100, 107–119

Heyer, T., Stamm, J., 2013. Levee reliability analysis using logistic regression models, abilities, limitations and practical considerations. Georisk 2013. 7:2, 77-87, DOI: 10.1080/17499518.2013.790734

Hossain, A. K. M. A., Easson, G., Hasan, K., 2006. Detection of Levee Slides Using Commercially Available Remotely Sensed Data. Journal of Environmental & Engineering Geoscience. 12, 235-246

Hossain A. K. M. A., Easson, G., 2012. Predicting shallow surficial failures in the Mississippi River levee system using airborne hyperspectral imagery. Geomat. Nat. Hazards Risk. 3, 55–78.

Hudson, P. F., Middelkoop, H., Stouthamer, E., 2008. Flood management along the Lower Mississippi and Rhine Rivers (The Netherlands) and the continuum of geomorphic adjustment, Geomorphology 101, 209–236.

Ibsen M.L., Brunsden D., 2004. Rainfall patterns and related landslide incidence in the Porretta-Vergato region, Italy. Landslides 1: 143–150

Jensen, J. R., 2007. Active & passive microwave remote sensing, in: remote sensing of the environment, an earth resource perspective, second ed. Pearson Education, Inc., NJ.

King, G., Zeng, L., 2001. Logistic regression in rare events data. Copy available at: http://gking.harvard.edu/files/gking/files/0s.pdf

Knighton, A.D., 1973. Riverbank erosion in relation to stream flow conditions, River Bollin-Dean, Cheshire. East Midlands Geographer 5, 416–426.

Lane, S.N., 1995. The dynamics of dynamic river channels. Geography 80 (2), 147–162. Mississippi Levee Board, 2009, Personal communication.

Lv, X., Yazici, B., Bennett, V., Zeghal, M., and Abdoun, T., 2013. Joint pixels InSAR for health assessment of levees in New Orleans. Proc., 2013 Geo-Congress: Stability and Performance of Slopes and Embankments III, Geotechnical Special Publication No. 231, San Diego, CA, March 3-6, ASCE, Reston, VA, 179-288.

Maciag, M. 2011. New levee database lists inspection ratings, other details. Governing, October 27 [online]. Available at http://www.governing.com/blogs/by-the-numbers/levee-database-lists-inspection-ratings-other-details.html

Nagata, N., Hosoda, T., Muramoto, Y., 2000. Numerical analysis of river channel processes with bank erosion, Journal of Hydraulic Engineering. 126, 243–252

National Weather Service Website, Access date: May, 2014: http://water.weather.gov/precip/about.php

NRC. 2012. Dam and levee safety and community resilience: A vision for future practice. National Research Council. The National Academies Press, Washington, DC.

Paudel, P. P., Omura, H., Kubota, T., Inoue, T., 2007. Spatio-temporal patterns of historical shallow landslides in a volcanic area, Mt. Aso, Japan. Geomorphology 88, 21-33.

Quinn, G. R., Keough, M. J., 2002. Experimental design and data Analysis for Biologists. Cambridge, UK: Cambridge University Press. ISBN 0-521-00976-6. (1st Ed.)

Reed, I., and X. Yu, 1990. Adaptive multiple-band CFAR detection of an optical pattern with unknown spectral distribution. IEEE Trans. Acoustics Speech and Signal Processing. 38, 1760–1770.

Reid, R. L., Nov. 2013. Defending New Orleans, Civil Engineering: The Magazine of the American Society of Civil Engineers, 48–67

Rosen, P., Hensley, S., Wheeler, K., Sadowy, G., Miller, T., Shaffer, S., Muellerschoen, R., Jones, C., Zebker, H., Madsen, S., 2006. UAVSAR: A new NASA airborne SAR system for science and technology research, IEEE Radar Conference, Verona, NY, April 24–27.

Saucier, R.T., 1994. Geomorphology and Quaternary Geologic History of the Lower Mississippi Valley, U.S. Army Corps of Engineers, Waterways Experiment Station.

Sehat, S., Vahedifard, F., Aanstoos, J. V., Dabbiru, L., Hasan, K., 2014a. Using in situ soil measurements for analysis of a polarimetric synthetic aperture radar-based classification of levee slump slides on the Lower Mississippi River, Eng. Geol., doi: 10.1016/j.enggeo.2014.07.007

Sehat, S., Vahedifard, F., Aanstoos, J. V., Dabbiru, L., Hasan, K., and Mooney, M. 2014b. Analysis of the Output from a Radar-Based Levee-Monitoring System Using In Situ Soil Data. Proc., Geo-Congress 2014: Geo-Characterization and Modeling for Sustainability, Geotechnical Special Publication No. 234, Atlanta, GA, February 23-26, 2014, ASCE, Reston, VA, 943-952.

Shankman, D., Smith, L.J., 2004. Stream channelization and swamp formation in the US Coastal Plain. Physical Geography 25, 22–38.

Sills, G. L., 1983. Long-term strength reduction and slough slides in Mississippi river levee: Vicksburg, U.S. Army Corps of Engineers, Vicksburg District.

Simon, A., Curini, A., Darby, S.E., Langendoen, E.J., 1999. Stream bank mechanics and the role of bank and near-bank processes in incised channels. In: Darby, S.E., Simon, A. (Eds.), Incised River Channels: Processes, Forms, Engineering and Management. John Wiley & Sons Ltd, London, pp. 123–152.

Stellman, C. M., Hazel, G. G., Bucholtz, F., Michalowicz, J. V., Stocker, A., Scaaf, W., 2000. Real-time hyperspectral detection and cuing, Opt. Eng., 39, 1928–1935.

United States Army Corps of Engineers, 2000. Design and construction of levees, Engineering Manual 1110-2-1913, U.S. Army Corps of Engineers.

United States Army Corps of Engineers, 2014. MR&T Project, July 2014. Available online at: http://www.mvd.usace.army.mil/Portals/52/docs/04_MRT_WEB.pdf

Uno, T., Morisugi, H., Sugii T., Ohashi, K., 1987. Application of a logit model to stability evaluation of river levees. Journal of Natural Disaster Science 9 (1), 61-77.

Zeghal, M., Abdoun, T., Exton, M., Mercado, V., Lv, X., Bennett, V., Yazici, B., Marr, A., 2013. Development of a multiscale monitoring and health assessment framework for effective management of levee infrastructure. Proc., 2013 Geo-Congress: Stability and Performance of Slopes and Embankments III, Geotechnical Special Publication No. 231, San Diego, CA, March 3-6, ASCE, Reston, VA, 1612–1621